NASA Technical Memorandum 83130

Methods for Estimating Pressure and Thermal Loads Induced by Elevon Deflections on Hypersonic-Vehicle Surfaces With Turbulent Boundary Layers

Louis G. Kaufman II and Charles B. Johnson

SEPTEMBER 1981

NASA

NASA Technical Memorandum 83130

Methods for Estimating Pressure and Thermal Loads Induced by Elevon Deflections on Hypersonic-Vehicle Surfaces With Turbulent Boundary Layers

Louis G. Kaufman II
Grumman Aerospace Corporation
Bethpage, New York

Charles B. Johnson
Langley Research Center
Hampton, Virginia

National Aeronautics
and Space Administration

**Scientific and Technical
Information Branch**

1981

CONTENTS

SUMMARY

Empirical-analytic methods are presented for estimating pressure and thermal loads induced by trailing-edge elevon deflections on adjacent surfaces of high-speed aircraft. The methods are applicable for turbulent-boundary-layer flows. The extent of the shock-wave—boundary-layer interaction region may be estimated adequately for all planar surfaces, but not for curved surfaces. However, knowing the extent of the three-dimensional interaction-flow region, pressure and heating distributions are adequately predictable. Heating magnification factors can be estimated using the methods presented herein once the pressure distributions are known.

INTRODUCTION

Interactions between the shock wave and boundary layer can appreciably affect the pressure and heating distributions on high-speed aircraft surfaces (refs. 1 to 16). The changing loads can affect aircraft stability and alter control effectiveness. Also, shock-wave—boundary-layer interaction flows can cause very high aerodynamic heating to occur at local surface regions. Any and all of these interaction-flow facets can compromise an aircraft design.

Except for simple two-dimensional (2-D) shapes, theoretical methods are not available for predicting either the changes in the surface pressure and thermal loads, or even the extent of the interaction. Not only is the three-dimensional (3-D) interaction-flow problem of more practical design importance, but it is further exacerbated by both the increased magnification of 3-D interaction-flow effects, and the lack of theoretical methods which would enable designers to predict these severe loads.

A photograph of a hypersonic research airplane model is shown in figure 1. Three-dimensional interaction-flow regions of paramount importance are expected in the engine inlet area and where shock waves from the fuselage, wings, fins, and elevons impinge on other surfaces of the aircraft. These interaction-flow regions can result in very large local-pressure and thermal peaks. Unfortunately, complex 3-D interaction-flow regions are not amenable to purely theoretical analyses (refs. 1 to 20).

Recourse must be made to empirical methods for the design of high-speed aircraft. A model of a hypersonic research airplane is shown in figure 1 and described in reference 6. Many organizations have done a great deal of work toward obtaining an understanding of the driving mechanisms of 3-D shock-wave—boundary-layer interaction flows (refs. 1 to 20). There have been many experimental investigations of these complex flows for both total-aircraft configurations (ref. 6) and also for fundamental model configurations representative of component parts of hypersonic aircraft. Examples of the latter are steps or fins mounted on flat plates or bodies of revolution (refs. 1 to 5 and 14).

The particular 3-D interaction flow addressed herein is that caused by deflecting trailing-edge elevons. The shock wave generated by the elevon can impinge on an aft fuselage surface and the shock-wave—boundary-layer interaction can result in a much larger region of disturbed surface pressures and heat-transfer distributions than anticipated using inviscid-flow analyses. Sketches of a typical hypersonic research airplane and a wing-elevon model, representative of the aft portion of the airplane, are shown in figure 2. Detailed data obtained for shock-wave interactions on the wing-elevon model (ref. 2) were very helpful in developing methods for estimating surface pressure and thermal loads in interaction-flow regions.

A related problem that has received much attention is that caused by fin generated shock waves incident to a boundary layer on an adjacent planar surface (refs. 8 and 12). The prime difference being the existence of a boundary layer upstream of the elevon hinge line. The similarity in the interaction flows prompts the use of both types of data in developing methods for estimating 3-D interaction-flow effects.

Many empirical methods that had been postulated for predicting surface pressure and thermal loads in 3-D interaction-flow regions were examined and compared with experimental results from other investigations. Portions of the more promising methods were modified slightly to improve agreement with an extended base of experimental data. The engineering methods presented herein were developed using extensive data from many sources. They are the best methods available for calculating pressure and thermal loads caused by shock waves, induced by elevon deflections, interacting with turbulent boundary layers on adjacent surfaces of hypersonic aircraft.

SYMBOLS

a	location of virtual origin along ξ-axis (eq. (7) and fig. 11), cm
b	semiminor axis defining hyperbola shown in figure 11, cm
b/a	slope of asymptote to separation location (eq. (6) and fig. 11)
c	empirical proportionality factor for peak heating (eq. (16))
HL	hinge line
h	heat-transfer coefficient, W/m^2-K
L	distance from plate leading edge to elevon hinge line (eq. (17)), cm
ℓ	separation length upstream of hinge line (fig. 7)
M	Mach number
n	exponent in expression for peak pressure magnification (eq. (13))
p	pressure, Pa

R	unit Reynolds number
x	streamwise distance measured downstream from where elevon-generated shock wave intersects wing surface (fig. 11), cm
x'	streamwise distance measured downstream from wing leading edge along surface of wing and elevon, cm
z	distance measured on end-plate surface upward from wing surface, cm
Δz	distance from shock wave to onset of pressure rise (eq. (8))
δ	boundary-layer thickness, cm
ε	elevon deflection angle, deg
θ	elevon shock-wave angle, deg
λ	angle from vertex of shock and x-axis to ray delineating maximum pressure or heating (eq. (10)), deg
ξ,ζ	shock-oriented, rectangular coordinate system (eq. (5) and fig. 11), cm

Subscripts:

incip	incipient
max	maximum value
peak	peak value
plat	plateau value
sep	separation
u	undisturbed
0	undisturbed flow value at hinge-line location
1	local flow conditions over wing and end-plate surfaces undisturbed by elevons
2	two-dimensional, oblique-shock value
∞	free-stream flow conditions

TYPES OF INTERACTION FLOWS

Two types of 3-D interaction flows induced by trailing-edge elevon deflections are sketched in figure 3. For smaller elevon deflection angles, the elevon-generated shock emanates from the hinge line (fig. 3(a)). For larger

deflection angles, the flow separates from the wing surface upstream of the hinge line, and a shock emanates from the separation line (fig. 3(b)). In both cases, the extent of the disturbance on the adjacent end-plate surface is far larger than would be anticipated using inviscid-flow analyses. The extent of the disturbed flow is shown in figure 3 by oil-accumulation lines.

WING AND ELEVON SURFACES

Pressure Distributions

Deflection-angle effects.- The local-flow compression angle is of first-order importance in determining the extent of 2-D turbulent boundary-layer separation ahead of elevons (flaps or ramps) and the resulting pressure distribution (refs. 21 to 29). The pressure rise required to cause 2-D turbulent boundary-layer separation may be expressed as a weak function of the local running-length Reynolds number. For a wide range of supersonic/hypersonic test conditions, the onset of separation ahead of elevons of sufficient chord length that the flow reattaches on the elevon surface (Chord length $>> \delta_0$) occurs for compression angles between 15° and 20°, and is predictable using Korkegi's criteria (ref. 13)

$$\frac{p_{incip}}{p_1} = \begin{cases} 1 + 0.3M_1^2 & \text{for } M_1 < 4.5 \\ 0.17M_1^{2.5} & \text{for } M_1 > 4.5 \end{cases} \qquad (1)$$

More recent methods show excellent correlations between incipient separation and friction coefficient. The small range of angles, the weak dependence on Reynolds number, the unsteadiness of turbulent separation, and the existence of 3-D eddies in 2-D separated flows are factors that seem to make superfluous more sophisticated means for predicting the onset of 2-D turbulent boundary-layer separation than that in equation (1) (refs. 21 to 29).

Example schlieren photographs of 2-D turbulent boundary-layer flows ahead of elevons are shown in figure 4 (ref. 2). The free-stream Mach number is 6 and the free-stream Reynolds number, based on the distance from the unswept wing leading edge to the elevon hinge line (64.14 cm), is 18.5 million (ref. 2). The local Mach number over the wing surface upstream of the elevon is 5.9. The shock wave emanating from the elevon hinge line changes slightly in shape from convex at low elevon angles to concave at larger elevon angles. A small region of separated flow in the vicinity of the hinge line is discernible only for a 30° elevon deflection. This is in agreement with the Korkegi criteria (ref. 13) shown in equation (1).

Sample pressure distributions, obtained in the Langley 20-Inch Mach 6 Tunnel (ref. 17), are compared with inviscid flow calculations in figure 5. Turbulent boundary layers do not separate significantly upstream of elevons for pressure

rises less than those calculable using equation (1) (i.e., no separation for $\varepsilon < 26^{\circ}$ based on inviscid-flow analysis and the conditions shown in fig. 5). As would be expected, the pressure distributions on the elevon surfaces are substantially different from those that would be calculated using inviscid-flow theory. For supersonic flows, the pressure on the flap remains less than the inviscid value for many boundary-layer thicknesses (refs. 21 to 29). For hypersonic flows however, there are generally "overshoots" in the flap-surface pressure distribution for sufficiently large deflection angles (i.e., angles large enough for separation). The loads on the flaps may be estimated assuming that the pressure attains the inviscid value at a surface distance of five boundary-layer thicknesses downstream of the hinge line (see "Wing and Control Loads" section).

Wing-sweep effects.- As long as the boundary layer is fully turbulent at all spanwise stations upstream of the hinge line, wing sweep has a negligible effect on the surface pressure distribution on the wing and elevon (ref. 17). There is no significant spanwise change in the pressure distribution. For trailing-edge controls that cause separation ahead of the hinge line, the extent of separation is uniform in length upstream of the hinge line for fully turbulent boundary layers. It is nonuniform if the boundary layer on the wing surface is transitional or laminar on the outboard portion of a swept wing where the chordwise Reynolds number is smaller (refs. 30 and 31).

Center-body and wing-tip-fin effects.- Vertical streamwise planar surfaces, such as end plates and tip fins, have little influence on the pressure distribution over the wing and elevon surfaces for attached flows (refs. 32 and 33). However, if the elevon angle is large enough to cause separation, end plates prevent venting of the vortical separated flow and the extent of turbulent boundary-layer separation ahead of trailing-edge elevons is more nearly uniform (ref. 32). For fully turbulent boundary-layer separation, the addition of end plates does not significantly extend the region of separated flow ahead of a trailing-edge elevon (compare figs. 83 and 84 in ref. 34). However, if the boundary layer is laminar or transitional near the separation location, the addition of end plates greatly enlarges the extent of separation, changes the effective surface shape, and results in far different pressure distributions than obtained without end plates (refs. 32 to 34).

A nonplanar center body (fuselage) has a negligible effect on the pressure distribution on the wing and elevon surfaces as long as there is no flow separation (ref. 32). However, even without separation, a fuselage causes an outflow of oil-flow streaks on the wing surface (ref. 32 and fig. 6(a)). When the elevon angle is large enough to cause turbulent boundary-layer separation, the fuselage shock and pressure fields cause large changes in the pressure distributions and extent of separation on the wing and elevon surfaces. As evidenced by the oil-flow photographs in figure 6, the maximum extent of separation ahead of the elevon is twice as large when the cylindrical body is attached to the wing as when the end plate is attached to the wing. As would be expected, oil accumulates at the juncture of the silicone rubber insert and the stainless steel wing, even though this juncture is thoroughly sealed. Nevertheless, the juncture is well upstream of the interaction region.

A planar end plate on the inboard portion of the wing, or a wing-tip fin, influences the separated flow slightly in its immediate vicinity (ref. 32 and fig. 6). However, a nonplanar fuselage causes a remarkable change in the separated-flow region, as evidenced by the oil-flow photographs shown in figure 6. The spanwise location of the maximum extent of separation occurs where the fuselage shock (calculated using the method described in ref. 35) intersects the elevon hinge line (fig. 6(c)). Corresponding to the larger extent of separation on the wing surface, reattachment occurs farther aft on the elevon surface. Although the spanwise location of this maximum extent of separation is predictable (occurring where the fuselage shock intersects the hinge line), there is no method for predicting the chordwise extent of separation. Recourse must be made to experimental results.

Wing and Control Loads

Wing loads.- Loads on the wing surface are unaffected unless the trailing-edge control causes the boundary layer to separate from the wing surface. Pressures are increased in the region of turbulent boundary-layer separation ahead of a control. A great amount of data have been reviewed in order to obtain methods for estimating the increased load on the wing surface when turbulent boundary-layer separation occurs upstream of the hinge line. Empirically, a dividing streamline angle of approximately 15° is observed for turbulent separation at Mach numbers from 2 to 10 and local running-length Reynolds numbers from 5 million to 50 million. Based on a review of extensive data (e.g., refs. 15, 16, and 30), the following equation was developed for estimating increased pressure levels on wings in regions of turbulent boundary-layer separation upstream of elevons:

$$\frac{p}{p_1} = 1.8 + 0.11M_1^2 \tag{2}$$

This empirical equation fits available data from many sources, and within the scatter of the data (20 percent) the pressure rise is nearly independent of local running-length Reynolds number for fully turbulent boundary-layer separation.

The extent of 2-D turbulent boundary-layer separation depends primarily on the flap deflection angle and the chord of the trailing-edge flap. The separated flow usually reattaches either on the flap surface or at the trailing edge of the flap. In the case where the flow reattaches on the flap surface, the extent of separation scales with the undisturbed boundary-layer thickness δ and the unit Reynolds number. In the case of reattachment at the flap trailing edge, the upstream extent of separation scales with the flap chord.

Ranges of upstream lengths of separation, nondimensionalized with respect to undisturbed turbulent boundary-layer thicknesses, are shown in figure 7 for a wide range of flow conditions (Mach numbers from 2 to 10 and local running-length Reynolds numbers from 5 million to 50 million) for cases where reattach-

ment occurs on the elevon surface (refs. 23 to 29). Generally, the normalized extent of separation increases with boundary-layer thickness and elevon deflection angle, but decreases with increasing Mach number and Reynolds number. Indeed, more detailed correlations of separation lengths with Reynolds number or local skin-friction coefficients have been presented in references 23 to 29. These more complex correlations should be consulted for more specific estimates of separation lengths for cases where reattachment occurs on the flap surface.

Whether the separated flow reattaches on the elevon surface or at the trailing edge of the elevon may be approximated with confidence by using inviscid-flow theory for sonic flow downstream of the elevon hinge line. When the calculated inviscid flow over the elevon surface is subsonic, reattachment occurs at the elevon trailing edge. In this case, the extent of separation may be estimated using a dividing streamline angle of 15° with reattachment at the elevon trailing edge. For smaller elevon angles, where the single-shock inviscid flow over the elevon surface would be supersonic, the extent of separation over the wing surface may be estimated roughly using figure 7. The extent of separation, along with the increased pressure on the wing surface in the separated flow region (eq. (2)), may be used to estimate the additional force on the wing surface.

Elevon loads.- When the elevon angle is sufficient to cause separation, the pressure on the elevon surface usually remains less than that which would be calculated inviscidly. Even in cases where there is no flow separation upstream of the hinge line, loads on the elevon surface vary from those that would be calculated using inviscid-flow methods. In general, the pressure on the elevon surface does not attain the inviscid pressure rise until 5 to 10 boundary-layer thicknesses downstream of the hinge line (refs. 23 to 29). However, for some instances of very high-speed fluid flow there is an "overshoot" in the surface pressure distribution (fig. 5 and ref. 36). In these cases the reflection waves caused by the shock wave emanating from the separation location should be considered. Otherwise, it is sufficient to assume that the pressure rise is linear to the inviscid value at a distance of 5 to 10 boundary-layer thicknesses downstream of the hinge line.

As evident in figure 5, the control force of an elevon is less than would be anticipated using inviscid-flow theory. This loss of control effectiveness is aggravated when the flow separates from the wing surface, increasing the load on the wing surface upstream of the hinge line (fig. 5).

Heat-Transfer Distributions

Deflection-angle effects.- Heat-transfer coefficients on the wing and undeflected elevon surfaces may be calculated accurately (to within approximately 10 percent) using any one of several methods (refs. 37 to 40). The heating on most of the wing surface is not changed as long as the elevon angle is insufficient to cause the boundary layer to separate (ref. 32). However, in detailed experiments with solid cast models of a hypersonic research airplane, Lawing (ref. 6) observed very high heating along elevon hinge lines even in the absence of significant flow separation.

Heat-transfer-coefficient distributions on the elevon surfaces may be estimated assuming a virtual origin for the turbulent boundary layer at the hinge line and using the measured or calculated pressure distribution. This simple method, however, does not account for the thickness of the upstream boundary layer and can lead to large discrepancies between calculated and measured heat-transfer coefficients on the elevon surface (ref. 32).

Heat-transfer coefficients increase in regions of turbulent boundary-layer separation (refs. 14, 15, 16, 28, and 32). The increased heating corresponds closely to the increased pressures on the wing surface for turbulent boundary-layer separation; i.e., the extent of increased heating is the same as the extent of increased pressures. Heat-transfer coefficients are largest near the forward position of the turbulent separated-flow region (fig. 8). The magnitude of these heating rates may be best estimated by comparing the design data with data gleaned from similar designs and flow conditions.

Maximum heat-transfer coefficients occur near reattachment of the separated flow on the elevon surface (fig. 8). For turbulent separated flows, the maximum heat-transfer coefficients at reattachment may be estimated using (refs. 18, 28, and 41 to 44)

$$\frac{h_{max}}{h_u} = \left(\frac{p_{max}}{p_1}\right)^{0.85} \tag{3}$$

This equation is helpful in estimating the order of magnitude of the maximum heat-transfer coefficient in most cases. However, measured peak heat-transfer coefficients can differ substantially from those calculated (ref. 40), as evidenced by the specific case shown in figure 8. As attested by many investigators (e.g., refs. 3, 5, 14, 15, and 16), there is considerable scatter and much uncertainty in heat-transfer data, particularly in separated-flow regions.

The heat-transfer coefficients indicated by the solid line in figure 8 were calculated using the measured pressure distribution over the elevon surface (refs. 32 and 40). As is the case for the distributions shown in figure 8, the actual location of maximum heating is frequently upstream of that calculated from the measured pressure distribution. Farther downstream of reattachment, however, the calculated heat-transfer coefficients agree fairly well with those measured experimentally.

Wing-sweep effects.- Lines of equal heat-transfer coefficients parallel the wing leading edge (refs. 32 and 45). As long as there is no flow separation, the heat-transfer distribution on the wing surface remains unchanged whether or not the elevon is deflected. When a turbulent boundary layer separates, the magnitude of the heat-transfer coefficient is increased in the separated-flow region. The area of increased heating is the same as that of increased pressure in the separated-flow region.

For swept wings, the heat-transfer coefficient is larger on the outboard portion of a deflected elevon. It is believed that this effect is due to the thinner boundary layer on the outboard portion of the swept wing (refs. 32 and 45). Since there may be a large difference between predicted and experienced values, within the broad range of Mach and Reynolds numbers stated previously, the most reliable expression currently available for predicting the maximum heat-transfer coefficient seems to be that given in equation (3).

Center-body and wing-tip-fin effects.- Fuselages and wing-tip fins have relatively little influence on the heat-transfer distribution on the wing surface as long as there is no shock impingement on the wing. Again, the region of increased heating is the same as the region of increased pressure. The largest heat-transfer coefficients occur just downstream of the onset of turbulent boundary-layer separation from the wing surface (refs. 32 and 45).

VERTICAL SURFACES

A deflected elevon, or trailing-edge flap induces pressure and thermal loads on an adjacent surface (such as an end plate, aft fuselage section, or vertical fin) over a much larger area than predicted by inviscid-oblique-shock analysis (see fig. 9). The 3-D interaction flow induced by a deflected elevon is somewhat similar to that induced by a fin mounted normal to a surface, the difference being the existence of a boundary layer on the wing surface upstream of the elevon, leading to thicker boundary layers on the elevon surface and the possibility of flow separation upstream of the elevon. Comprehensive discussions of the nature of 3-D flow interactions are presented in references 5, 7, 8, 10, 11, 12, and 20.

Interaction-Flow Region

Incipient separation.- Hayes (ref. 8), Korkegi (ref. 13), and others have pointed out that 3-D flow separation occurs much more readily than 2-D flow separation. The turbulent boundary layer on a surface subjected to a skewed shock wave will separate for streamwise pressure rises of

$$\frac{p_{incip}}{p_1} \approx 1.65 \tag{4}$$

This value (1.65) is simply an average of the values presented by Hayes in reference 8 (1.8) and by Korkegi in reference 13 (1.5). The onset of 3-D flow separation is difficult to ascertain and has little effect on the loads on the end-plate surface until the pressure rise exceeds a factor of two.

Pressure and thermal-load characteristics.- References 8, 41, and 42 have proposed analytical methods for estimating pressure and heating distributions induced on a planar surface by a vertical fin with a sharp leading edge. Except for the boundary layer on the wing surface upstream of the elevon, their geom-

etry is similar to that discussed herein, with the fin simulating the elevon and the flat plate simulating the vertical end plate. Their methods are based on experimental results and correlations of empirical data from many sources.

Sketches of interaction-flow regions on the end-plate surface and the corresponding pressure and heat-transfer-coefficient distributions, as depicted by Hayes (ref. 8), are shown in figure 10. Surface streamlines, as evidenced by oil-flow investigations, start to curve and the pressure and heat-transfer coefficient start to rise at the onset of the interaction region. At separation, the pressure approaches a plateau value whereas the heat-transfer coefficient attains a local maximum value. At the shock location, the pressure dips to a local minimum value, then increases to a peak value near the elevon surface as shown in figure 10 (refs. 8, 12, and 41). Hayes (ref. 8) and Scuderi (ref. 41) observed that peak heat-transfer coefficients occur quite close to where the pressure attains its peak value, several boundary-layer thicknesses downstream of the elevon hinge line (fin leading edge).

Extent of separation and interaction-flow regions.- Hayes (ref. 8) presents a method for estimating the location of separation that is found to be reliable. A shock-oriented coordinate system (ξ,ζ) is used with a virtual origin upstream of the shock wave emanating from the separation location ahead of the elevon (fig. 11). The location of separation on the adjacent end plate is well approximated by a branch of the hyperbola indicated in figure 11. Using the shock-oriented coordinate system and data from many sources, Hayes found that the data followed a hyperbola

$$\zeta^2 = \left(\frac{b}{a}\right)^2 (\xi^2 - a^2) \tag{5}$$

as a good approximation for the location of separation.

The slope of the asymptote to the separation location, gleaned from the results of many experiments, was presented in figure 10 of reference 8. Using the suggested parameter $(M_1 \sin \theta)$, a simple equation was fit to the data presented by Hayes

$$\frac{b}{a} = 0.442(M_1 \sin \theta) - 1.262 + \frac{0.968}{(M_1 \sin \theta)} + \frac{0.127}{(M_1 \sin \theta)^2} \tag{6}$$

where θ is the shock-wave angle and M_1 is the Mach number of the local undisturbed flow. The location of the virtual origin a along the ξ-axis may be estimated using the following equation, which is simply another curve fit to the extensive data presented by Hayes (ref. 8):

$$a = 3 + \frac{5}{(M_1 \sin \theta - 1.3)^{1.5}} \tag{7}$$

where the distance a is in centimeters (curve fit to fig. 11 of ref. 8).

The location of the onset of the interaction-flow region depends on both the shock strength and the local-boundary-layer thickness. Scuderi (ref. 41) relates the outboard extent of the beginning of the interaction pressure rise to the location of the shock wave, the pressure rise (governed by the elevon deflection angle ε), and the boundary-layer thickness δ

$$\frac{\Delta z}{\delta} = (0.0115\varepsilon + 0.1)\frac{x}{\delta} + 0.14\varepsilon \tag{8}$$

where ε is in degrees and x is the streamwise distance downstream of where the elevon generated shock wave intersects the wing surface. This expression is generally valid and simple to use. The distance along the z-axis from the shock wave to the onset of the pressure rise is Δz measured downstream of where the shock wave intersects the wing surface (figs. 10 and 11). Hayes (ref. 8) presents data relating the pressure rise from the onset of the disturbed region to the location of separation, with the extent of the distance between the lines labeled "Onset" and "Separation" in figure 10. The overpressure in this region, which averages approximately $0.5(p_{plat} - p_1)$, adds little to the induced side force on the end plate. It may be accurately approximated using a linear pressure distribution from p_1 at the onset location to p_{plat} at the separation location.

Separation locations calculated using Hayes' method (ref. 8) agree well with experimental observations (ref. 32) shown in figure 12. The rectangular coordinate system used in equations (5) to (7) and in figure 11 is shock wave oriented. The transformation equations are

$$\left.\begin{aligned} x &= \xi \cos \theta - \zeta \sin \theta - a \cos \theta \\ z &= \xi \sin \theta + \zeta \cos \theta - a \sin \theta \end{aligned}\right\} \tag{9}$$

where θ is the shock-wave angle and the x,z origin is where the shock wave intersects the wing surface (not necessarily at the hinge line).

Locations of peak pressure and heating.- Peak pressure ratios and maximum heat-transfer-coefficient ratios occur near the elevon surface. Hayes (ref. 8) notes that for values of $\frac{x}{\delta} < 10$, the ray of peak pressure ratio is closer

to the elevon surface than the ray of maximum heat-transfer ratio. Scuderi (ref. 41) has correlated much data and presents

$$\left.\begin{aligned} \lambda - \varepsilon &= 0.28(\theta - \varepsilon) \quad \text{for peak pressure} \\ \lambda - \varepsilon &= 0.24(\theta - \varepsilon) \quad \text{for peak heating} \end{aligned}\right\} \tag{10}$$

where λ is the angle from the vertex of the shock wave and x-axis to the ray delineating the peak pressure or heating. Evident from equation (10), both of these rays are close to the elevon surface. For $M_1 = 5.9$ and $\varepsilon = 20^\circ$, $\theta = 28.6^\circ$. From equation (10), $(\lambda - \varepsilon)_{\text{peak pressure}} = 2.4^\circ$ and $(\lambda - \varepsilon)_{\text{peak heating}} = 2.1^\circ$. These are indeed close to the elevon surface.

Pressure Distributions

Plateau and separation pressure rises.- Hayes (ref. 8) and Scuderi (ref. 41) observed that pressure rises in the interaction-flow region correlate well with $(M_1 \sin \theta)$. A simple polynomial curve was fit to the data presented by Hayes in figure 7 of reference 8. The plateau pressure may be estimated using

$$\frac{p_{plat}}{p_1} = 0.41 + 0.91(M_1 \sin \theta) - 0.06(M_1 \sin \theta)^2 \tag{11}$$

The pressure rise at the separation location may be estimated using data presented by Hayes (ref. 8)

$$p_{sep} = 0.73 p_{plat} \tag{12}$$

Scuderi (ref. 41) observed an initial peak pressure rise somewhat higher in value than the plateau pressure. This local pressure peak adds little to the side force acting on the end plate. In the experiments for $M_1 = 5.9$, no initial peak pressure higher than the plateau pressure was apparent (ref. 17). Neither Hayes (ref. 8) nor Korkegi (ref. 12) reported an initial peak pressure prior to the plateau-pressure region.

Shock and peak pressures in inner-flow region.- The inner-flow region extends from the elevon surface to the shock wave (refs. 8 and 12). There is a dip in the pressure distribution at the shock wave and then the pressure rises to a peak value near the elevon surface (refs. 8, 12, and 17) (fig. 13). The minimum pressure at the shock is difficult to ascertain, and the sparse data are difficult to correlate. The dip in the pressure apparently depends on shock strength, distance downstream of the shock vertex, and boundary-layer thickness. Although there is no convenient expression for the minimum pressure at the shock wave, the extent of the region is quiet small and the pressure ratio is bounded

by the plateau-pressure ratio and unity. The effect of this small dip in pressure on the side force exerted on the end plate is negligible.

The magnitude of the peak pressure ratio p_{peak}/p_1 also depends on shock strength, distance downstream, and boundary-layer thickness. However, the value of this ratio is well documented. The peak pressure is estimable using reference 8

$$\frac{p_{peak}}{p_1} = (M_1 \sin \theta)^n \tag{13}$$

by simply curve fitting equations to Hayes' data

$$n = \begin{cases} 1.4 + \dfrac{1.1(x/\delta)}{3.8 + (x/\delta)} & \text{for } x < 38\delta \\ 2.4 & \text{for } x > 38\delta \end{cases} \tag{14}$$

Scuderi (ref. 41) also observed that the peak pressure increases with both shock strength and increased values of x/δ. His results agree with those calculated using equations (13) and (14) and also with the results for $M_1 = 5.9$ (ref. 17).

Finally, at the elevon surface the pressure approaches the oblique-shock value obtained from reference 46 (refs. 8, 12, and 41)

$$\frac{p_2}{p_1} = \frac{7(M_1 \sin \theta)^2 - 1}{6} \tag{15}$$

Close to the elevon hinge line ($x < 5\delta$), the peak pressure may be less than the pressure at the elevon surface. Further downstream, the peak pressure exceeds the pressure at the elevon surface.

Sample comparison.- A pressure-ratio distribution on the end-plate surface along a vertical line (calculated using the analytic method described in eqs. (5) to (15)), is compared with experimental data in figure 13. The particular case plotted is for $M_1 = 5.9$, $\varepsilon = 20^\circ$, $x = 7.6$ cm, and $\delta = 0.86$ cm. The value of the pressure ratio at the elevon surface is that given by using equation (15). The peak pressure ratio is obtained using equations (13) and (14) and the location of the peak pressure x_{peak} is obtained using equation (10). An S-shaped curve is faired between these two points in figure 13. The pressure on the end-plate surface, going away from the elevon, then dips to a minimum value ($0.5(p_{plat} + p_1)$) at the inviscid-shock location (which is calculated using ref. 46). The pressure then rises to the plateau value (eq. (11)) and is essen-

tially constant outboard to the separation location (calculated using eqs. (5) to (7)). Another S-curve represents the pressure-ratio distribution from the location of separation to the undisturbed value at the onset of the disturbance, given by equation (8). Considering the complexity of the 3-D interaction-flow problem and the simplicity of the proposed analytical method, the agreement is quite adequate.

Wing-sweep and tip-fin effects.- As long as the boundary layer is turbulent upstream of the elevon, wing sweep has no effect on the pressure on the end-plate surface. Tip fins at the outboard edge of the elevon usually have no effect on the end-plate-surface pressure distribution (refs. 17 and 32). For very-low-aspect-ratio elevons, relatively large tip fins may result in more extensive separation ahead of elevons. This would shift forward the location of the interaction-flow region on the end-plate surface.

Force on End Plate

Elevons influence a much larger area of the end-plate surface than would be predicted using simple 2-D inviscid-flow analysis. However, the average pressure rise in this region is considerably less than that downstream of a 2-D oblique shock wave. In the experiments for $M_\infty = 6$, the total side force induced on the end-plate surface by 10° to 30° elevons varied from 85 to 98 percent of the force that would be predicted using the 2-D flow analysis of equation (15) (refs. 2 and 32).

Heat-Transfer Distributions

Peak heat-transfer coefficients.- The maximum value of the heat-transfer-coefficient ratio, induced by the elevon on the end-plate surface, may be estimated by using (from ref. 8)

$$\frac{h_{peak}}{h_u} = c(M_1 \sin\theta - 1) + 0.75$$

where

$$c = \begin{cases} 1 + \frac{2}{3}\left(\frac{x}{\delta}\right) & \text{for } x < 5\delta \\ 4.3 + 0.01\left(\frac{x}{\delta}\right) & \text{for } x > 5\delta \end{cases} \qquad (16)$$

These linear expressions for c were obtained by simply fairing lines through the data presented by Hayes in reference 8.

An alternate expression for the value of the maximum heat-transfer-coefficient ratio, expounded by Scuderi (ref. 41), is

$$\frac{h_{peak}}{h_u} = \left[1.2\left(\frac{p_{peak}}{p_1}\right)^{0.85} + 0.2\right]\left(1 + \frac{x}{L}\right)^{0.2} \tag{17}$$

where x is measured downstream from where the elevon generated shock wave intersects the wing surface and L is the distance from the plate leading edge to the elevon hinge line.

Finally, another expression for the maximum heating amplification that is in agreement with data from many sources was presented fairly recently by Neumann and Hayes (ref. 5)

$$\frac{h_{peak}}{h_u} = \left(\frac{p_{peak}}{p_1}\right)^{0.8} \tag{18}$$

Sample comparisons.- Peak heat-transfer values were calculated using equations (16) to (18) and compared with experimental results for an example case (fig. 14). The example case chosen was an end plate adjacent to a 20° elevon (refs. 2 and 45). The elevon hinge line is located 55 cm downstream of the wing leading edge (L = 55 cm). The boundary-layer thickness, measured from profile schlieren flow photographs when the end plate was not attached, is 0.86 cm at a station 7.6 cm downstream of the elevon hinge line (ref. 45). This measured boundary-layer thickness agrees with the value calculated by the Anderson and Lewis boundary-layer code, using a measured pressure distribution as input (ref. 37). The local Mach number of the flow over the flat-plate wing, upstream of the hinge line, is 5.9 (ref. 45). The peak pressure ratio, calculated using equations (13) and (14), is approximately 9.5 (shown in fig. 13).

These values, used in equations (16), (17), and (18) to calculate predicted peak heating yield the following results:

Equation no.:	(16)	(17)	(18)
h_{peak}/h_u:	8.76	8.55	6.06

The equation proposed by Neumann and Hayes (ref. 5) gives results close to the experimental values for the example case shown in figure 14.

Wing-sweep and tip-fin effects.- Heat-transfer-coefficient distributions on the end plate are similar to pressure distributions on the end plate in that they are not affected by wing sweep as long as the boundary layer is turbulent upstream of the elevon (refs. 32 and 45). For low-aspect-ratio elevons, large tip fins may result in a larger region of separated flow ahead of the elevon; this would result in a forward shift of the shock and the increased-heating

region on the end-plate surface. For large-aspect-ratio elevons, or for elevon deflection angles less than those required to cause separation, tip fins at the outboard edge of the elevons have no effect on the heat-transfer distributions on the end-plate surface.

Cylindrical body.- Neumann and Hayes (ref. 5) present extensive interaction-flow data obtained for unswept fins mounted on ogive cylinders. They find that the location of peak heating is quite close to the fin on the cylindrical surface, and is similar to the location of peak heating on a flat-plate-fin configuration (eq. (10)). The magnitude of the peak heating on a cylindrical surface is similar to that for a flat-plate-fin configuration, and may be estimated using equation (18) (ref. 5).

In figures 15 and 16, interaction-flow regions on an end plate and a cylindrical body are compared (ref. 45). The interaction-flow data are for $M_1 = 5.9$ and an elevon deflection angle of 20°. The extent of the interaction-flow region is larger on the cylindrical body than on the planar end plate, and the demarcation line on the cylindrical-body surface is curved. In agreement with the results presented by Neumann and Hayes (ref. 5), the locations of maximum heating are approximately the same for the cylindrical body and the planar end plate. The heating magnification is larger for the cylindrical body as a result of the undisturbed heat-transfer coefficient on the cylindrical body being somewhat less than that on the end plate (ref. 45).

CONCLUDING REMARKS

Pressure and thermal loads induced by trailing-edge elevons on high-speed aircraft surfaces can differ substantially from those that would be anticipated using inviscid-flow analyses. Even without flow separation, the control load on the elevon is less than that calculated inviscidly. The extent of the interaction-flow region on an adjacent fuselage surface is much larger than predictable using inviscid-flow analyses, but the total side force is less.

The methods presented herein are adequate for preliminary estimates of the forces induced on adjacent planar surfaces by deflected elevons. The extent of the interaction-flow region, as well as surface pressure distributions, can be predicted for planar wing, elevon, and end-plate surfaces. For nonplanar configurations, such as a cylindrical fuselage adjacent to the elevon in lieu of a planar end plate, there are no analytical methods for predicting the extent of the 3-D interaction-flow region.

Heating magnification factors may be estimated, using the methods presented herein, as long as the pressure distributions are known. Regions of maximum heating, as well as their magnitudes, are estimable using the methods given herein.

Langley Research Center
National Aeronautics and Space Administration
Hampton, VA 23665
June 26, 1981

REFERENCES

1. Cassel, L. A.; and Jarrett, T. W.: Hypersonic Flow Over Small Span Flaps in a Thick Turbulent Boundary Layer. AIAA-80-1475, July 1980.

2. Johnson, Charles B.; and Kaufman, Louis G., II: High-Speed Interference Heating Loads and Pressure Distributions Resulting From Elevon Deflections. J. Aircr., vol. 17, no. 3, Mar. 1980, pp. 175-181.

3. Hung, F. T.; and Clauss, J. M.: Three-Dimensional Protuberance Interference Heating In High Speed Flow. AIAA-80-0289, Jan. 1980.

4. Horstman, C. C.; and Hung, C. M.: Computation of Three-Dimensional Turbulent Separated Flows at Supersonic Speed. AIAA J., vol. 17, no. 11, Nov. 1979, pp. 1155-1156.

5. Neumann, R. D.; and Hayes, J. R.: Aerodynamic Heating in the Fin Interaction Region of Generalized Missile Shapes at Mach 6 (Modular Missile Test Program) - Wind Tunnel Tests. AFFDL-TR-79-3066, May 1979. (Available from DTIC as AD A071 573.)

6. Lawing, Pierce L.: Configuration Heating for a Hypersonic Research Airplane Concept Having a 70° Swept Double-Delta Wing. NASA TP-1143, 1978.

7. Three Dimensional and Unsteady Separation at High Reynolds Numbers. AGARD-LS-94, Feb. 1978.

8. Hayes, James R.: Prediction Techniques for the Characteristics of Fin Generated Three Dimensional Shock Wave Turbulent Boundary Layer Interactions. AFFDL-TR-77-10, U.S. Air Force, May 1977. (Available from DTIC as AD A042 024.)

9. Hearth, Donald P.; and Preyss, Albert E.: Hypersonic Technology - Approach to an Expanded Program. Astronaut. & Aeronaut., vol. 14, no. 12, Dec. 1976, pp. 20-37.

10. Peake, D. J.: Three-Dimensional Swept Shock/Turbulent Boundary-Layer Separations With Control by Air Injection. LR-592 (NRC No. 15579), Natl. Res. Counc. of Canada, July 1976.

11. Schepers, H. J.: Flow and Heat Transfer Measurements in Corner Regions at Hypersonic Speeds. ESA TT-302, 1976. (Available from NTIS.)

12. Korkegi, R. H.: On the Structure of Three-Dimensional Shock-Induced Separated Flow Regions. AIAA J., vol. 14, no. 5, May 1976, pp. 597-600.

13. Korkegi, R. H.: Comparison of Shock-Induced Two- and Three-Dimensional Incipient Turbulent Separation. AIAA J., vol. 13, no. 4, Apr. 1975, pp. 534-535.

14. Korkegi, Robert H.: Survey of Viscous Interactions Associated With High Mach Number Flight. AIAA J., vol. 9, no. 5, May 1971, pp. 771-784.

15. Ryan, B. M.: Summary of the Aerothermodynamic Interference Literature. Tech. Note 4061-160, Naval Weapons Center (China Lake, Calif.), Apr. 1969.

16. Chilcott, R. E.: A Review of Separated and Reattaching Flows With Heat Transfer. Int. J. Heat & Mass Transfer, vol. 10, no. 6, June 1967, pp. 783-797.

17. Kaufman, Louis G., II; and Johnson, Charles B.: Pressure Distributions Induced by Elevon Deflections on Swept Wings and Adjacent End-Plate Surfaces at Mach 6. NASA TM X-3470, 1977.

18. Johnson, Charles B.; and Kaufman, Louis G., II: Incident Shock Interactions With Boundary Layers. J. Spacecr. & Rockets, vol. 12, no. 6, June 1975, pp. 327-328.

19. Edwards, A. J.: Heat Transfer Distributions on a 70° Delta Wing With Flap-Induced Separation. I. C. Aero Rep. 75-01, Imperial College of Science and Technology (London), Mar. 1975.

20. Goldberg, Theodore J.: Three-Dimensional Separation for Interaction of Shock Waves With Turbulent Boundary Layers. AIAA J., vol. 11, no. 11, Nov. 1973, pp. 1573-1575.

21. Paynter, G. C.: Analysis of Weak Glancing Shock/Boundary-Layer Interactions. J. Aircr., vol. 17, no. 3, Mar. 1980, pp. 160-166.

22. Modarress, D.; and Johnson, D. A.: Investigation of Turbulent Boundary-Layer Separation Using Laser Velocimetry. AIAA J., vol. 17, no. 7, July 1979, pp. 747-752.

23. Settles, Gary S.; Fitzpatrick, Thomas J.; and Bogdonoff, Seymour M.: Detailed Study of Attached and Separated Compression Corner Flowfields in High Reynolds Number Supersonic Flow. AIAA J., vol. 17, no. 6, June 1979, pp. 579-585.

24. Horstman, C. C.; Settles, G. S.; Vas, I. E.; Bogdonoff, S. M.; and Hung, C. M.: Reynolds Number Effects on Shock-Wave Turbulent Boundary-Layer Interactions. AIAA J., vol. 15, no. 8, Aug. 1977, pp. 1152-1158.

25. Roshko, A.; and Thomke, G. J.: Flare-Induced Interaction Lengths in Supersonic, Turbulent Boundary Layers. AIAA J., vol. 14, no. 7, July 1976, pp. 873-879.

26. Law, C. Herbert: Supersonic Shock Wave Turbulent Boundary-Layer Interactions. AIAA J., vol. 14, no. 6, June 1976, pp. 730-734.

27. Settles, Gary S.; Bogdonoff, Seymour M.; and Vas, Irwin E.: Incipient Separation of a Supersonic Turbulent Boundary Layer at High Reynolds Numbers. AIAA J., vol. 14, no. 1, Jan. 1976, pp. 50-56.

28. Hankey, W. L., Jr.; and Holden, M. S.: Two-Dimensional Shock Wave-Boundary Layer Interactions in High Speed Flows. AGARD-AG-203, June 1975.

29. Law, C. Herbert: Supersonic, Turbulent Boundary-Layer Separation. AIAA J., vol. 12, no. 6, June 1974, pp. 794-797.

30. Kaufman, Louis G., II; and Freeman, L. Michael: Separation Ahead of Controls on Swept Wings. ARL TR 75-0134, U.S. Air Force, June 1975.

31. Kaufman, Louis G., II; and Freeman, L. M.: Separation Ahead of Steps on Swept Wings. J. Aircr., vol. 13, no. 12, Dec. 1976, pp. 1016-1017.

32. Kaufman, Louis G., II; and Johnson, Charles B.: Pressure and Thermal Distributions on Wings and Adjacent Surfaces Induced by Elevon Deflections at Mach 6. NASA TP-1356, 1979.

33. Kaufman, L. G., II; Meckler, L.; and Hartofilis, S. A.: An Investigation of Flow Separation and Aerodynamic Controls at Hypersonic Speeds. J. Aircr., vol. 3, no. 6, Nov.-Dec. 1966, pp. 555-561.

34. Kaufman, Louis G., II: Pressure and Heat Transfer Measurements for Hypersonic Flows Over Expansion Corners and Ahead of Ramps - Part II: Mach 5 Pressure Data for Flows Ahead of Ramps. ASD-TDR-63-679, Part II, U.S. Air Force, Sept. 1963. (Available from DTIC as AD 421 859.)

35. Marconi, Frank; Salas, Manuel; and Yaeger, Larry: Development of a Computer Code for Calculating the Steady Super/Hypersonic Inviscid Flow Around Real Configurations. Volume I - Computational Technique. Volume II - Code Description. NASA CR-2675, 1976.

36. Hill, W. G., Jr.: Analysis of Experiments on Hypersonic Flow Separation Ahead of Flaps Using a Simple Flow Model. RM-383, Grumman Aircraft Eng. Corp., Nov. 1967.

37. Anderson, E. C.; and Lewis, C. H.: Laminar or Turbulent Boundary-Layer Flows of Perfect Gases or Reacting Gas Mixtures in Chemical Equilibrium. NASA CR-1893, 1971.

38. Harris, Julius E.: Numerical Solution of the Equations for Compressible Laminar, Transitional, and Turbulent Boundary Layers and Comparisons With Experimental Data. NASA TR R-368, 1971.

39. Hopkins, Edward J.; Keener, Earl R.; and Louie, Pearl T.: Direct Measurements of Turbulent Skin Friction on a Nonadiabatic Flat Plate at Mach Number 6.5 and Comparisons With Eight Theories. NASA TN D-5675, 1970.

40. Johnson, Charles B.; and Boney, Lillian R.: A Simple Integral Method for the Calculation of Real-Gas Turbulent Boundary Layers With Variable Edge Entropy. NASA TN D-6217, 1971.

41. Scuderi, L. F.: Expressions for Predicting 3-D Shock Wave-Turbulent Boundary Layer Interaction Pressures and Heating Rates. AIAA Paper 78-162, Jan. 1978.

42. Neumann, R. D.; and Token, K. H.: Prediction of Surface Phenomena Induced by Three Dimensional Interactions on Planar Turbulent Boundary Layers. IAF Paper 74-058, Sept.-Oct. 1974.

43. Hung, F. T.: Interference Heating Due to Shock Wave Impingement on Laminar Boundary Layers. AIAA Paper No. 73-678, July 1973.

44. Holden, M. S.: Shock Wave-Turbulent Boundary Layer Interaction in Hypersonic Flow. AIAA Paper No. 72-74, Jan. 1972.

45. Johnson, Charles B.; and Kaufman, Louis G., II: Heat Transfer Distributions Induced by Elevon Deflections on Swept Wings and Adjacent Surfaces at Mach 6. NASA TM-74045, 1978.

46. Ames Research Staff: Equations, Tables, and Charts for Compressible Flow. NACA Rep. 1135, 1953. (Supersedes NACA TN 1428.)

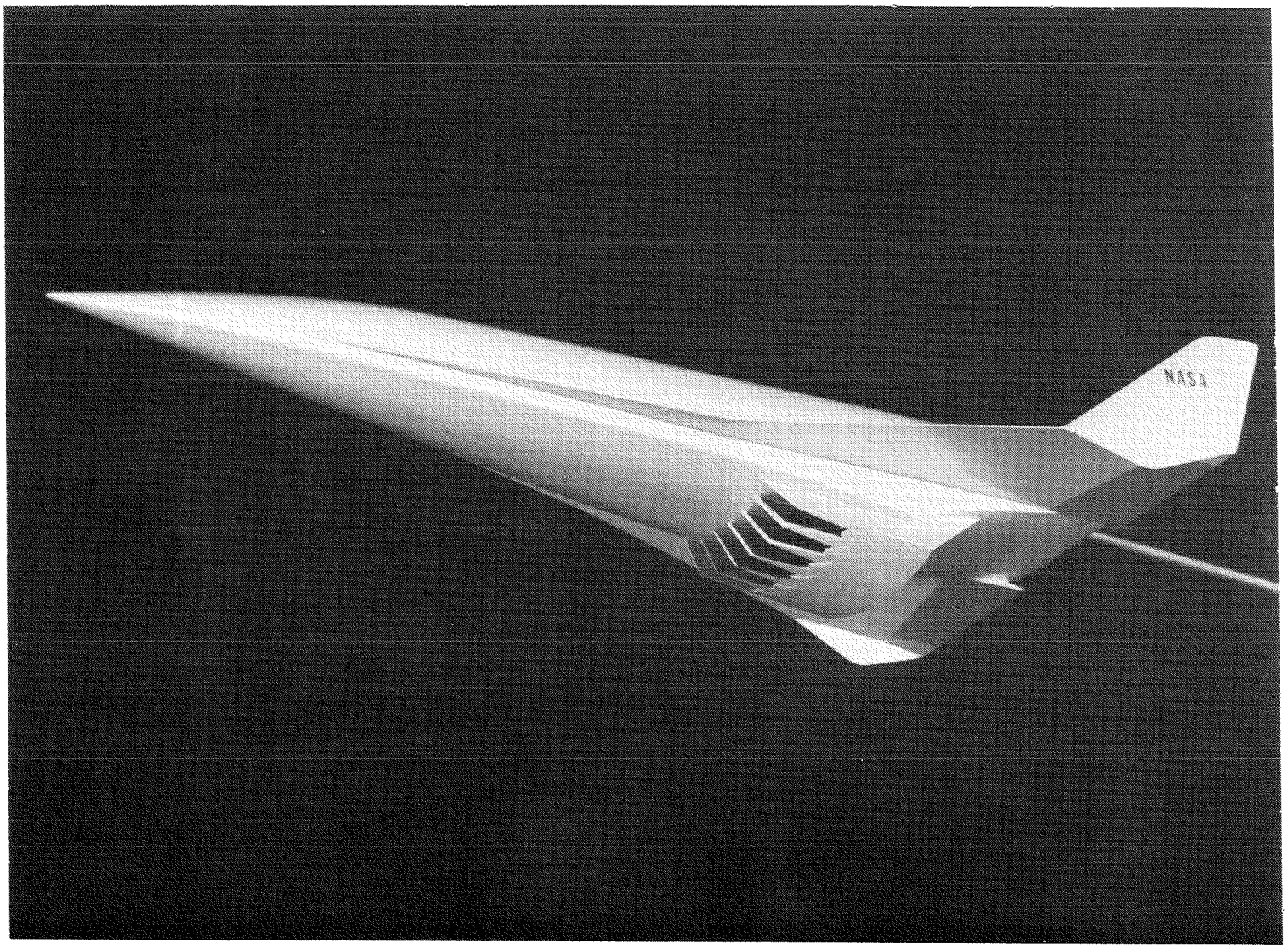

L-72-9142

Figure 1.- Model of hypersonic research airplane.

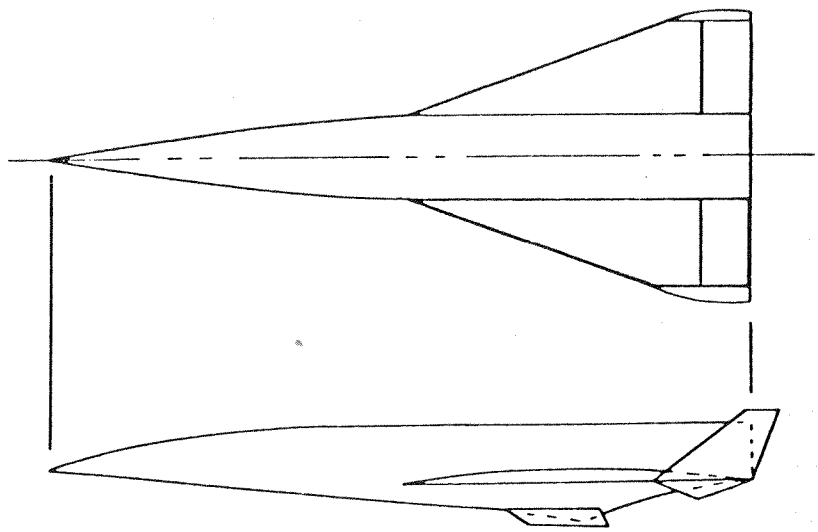

Hypersonic research airplane

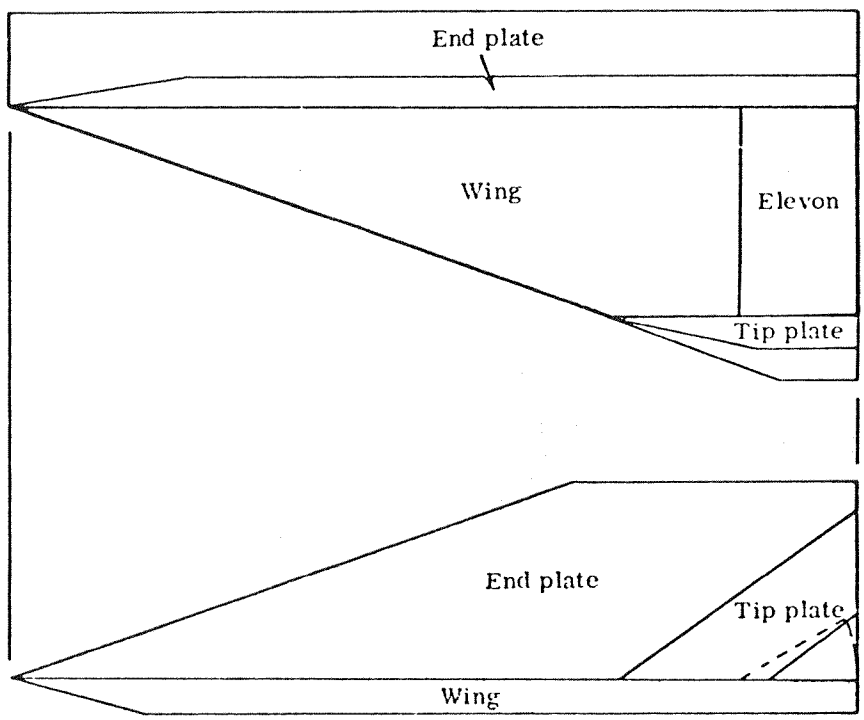

Wing-elevon model

Figure 2.- Outlines of typical hypersonic research airplane and wing-elevon model.

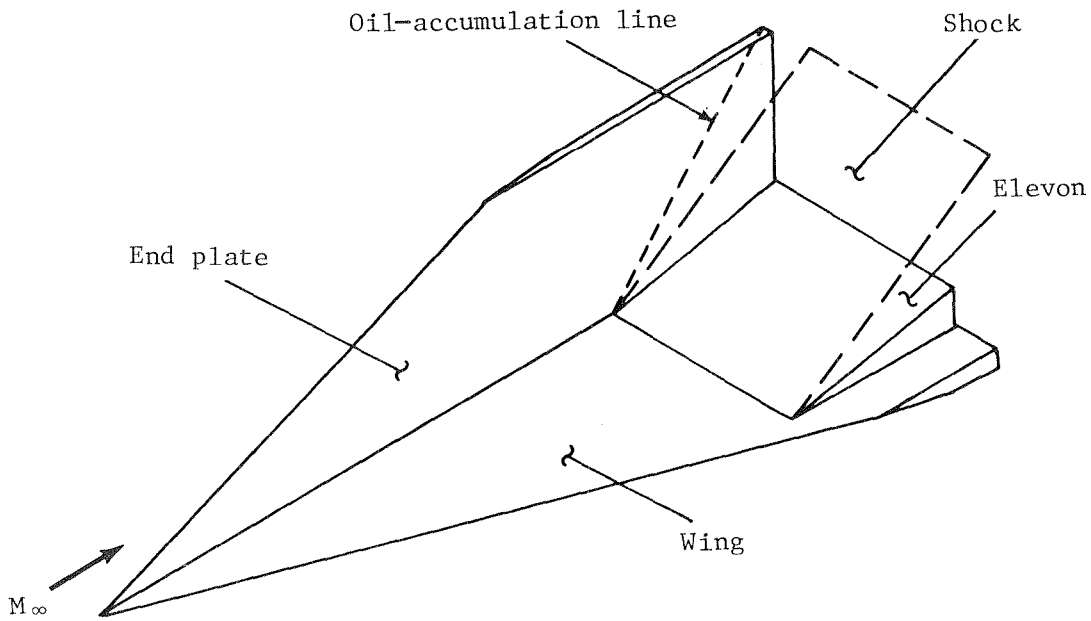

(a) No separation upstream of elevon hinge line.

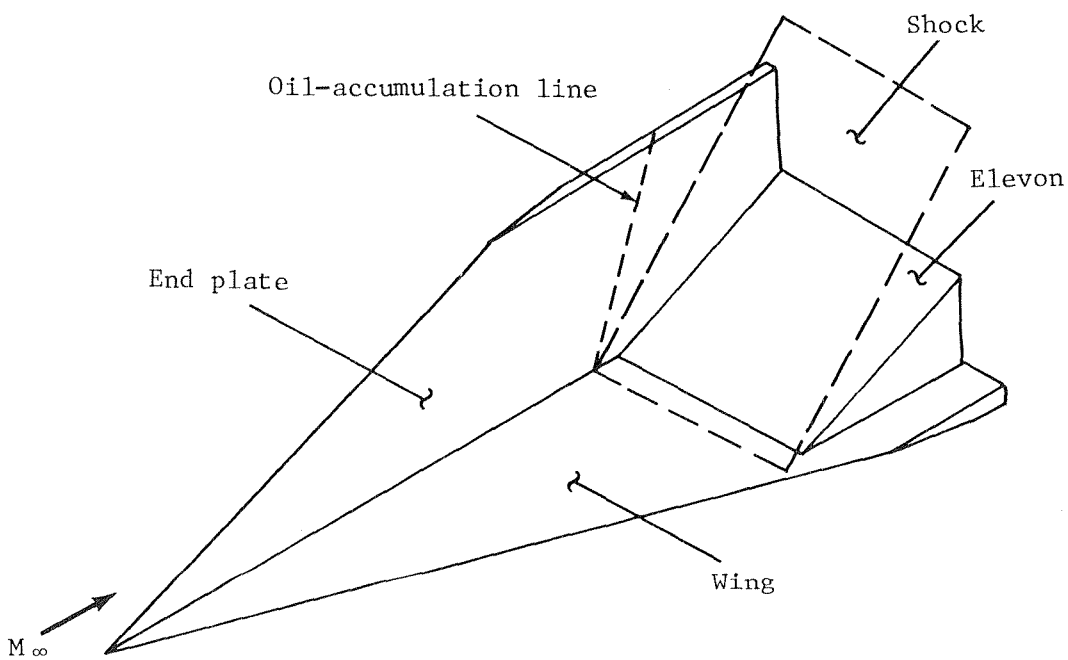

(b) Separated flow upstream of elevon hinge line.

Figure 3.- Three-dimensional interaction-flow models.

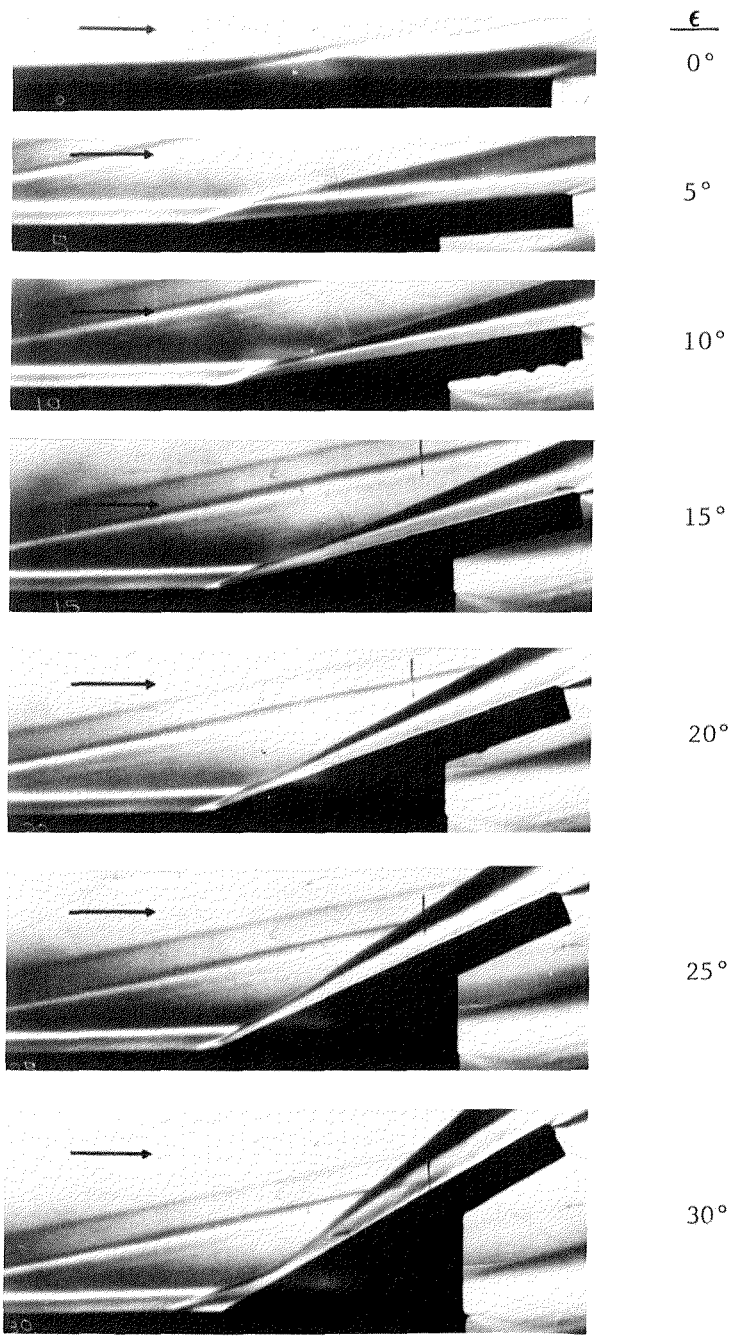

Figure 4.- Profile schlieren flow photographs of unswept-wing elevons for $M_\infty = 6$ with turbulent boundary layer (ref. 2).

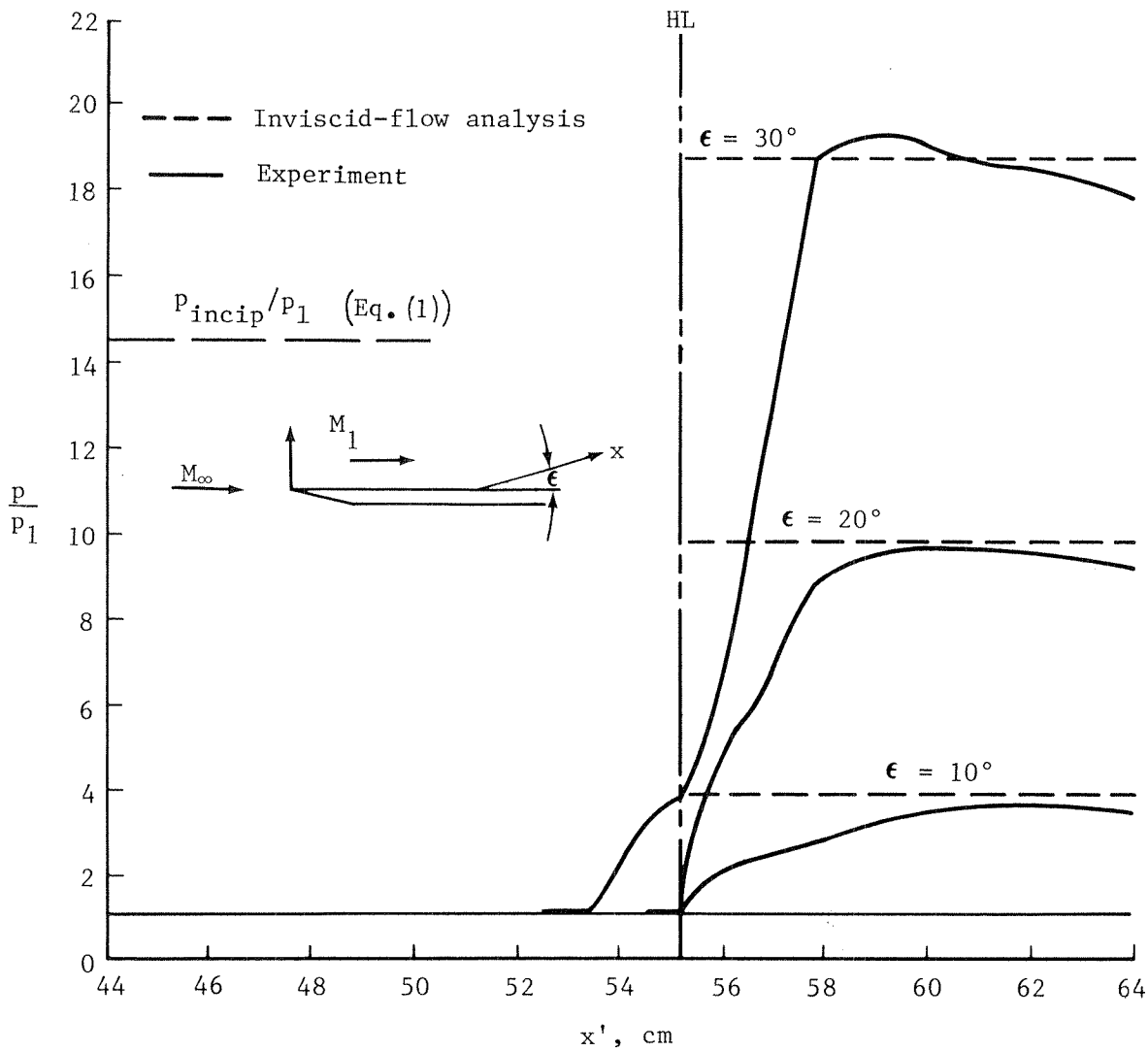

Figure 5.- Streamwise pressure-ratio distributions on upswept wing and elevon surfaces along elevon midspan line. $M_1 = 5.9$.

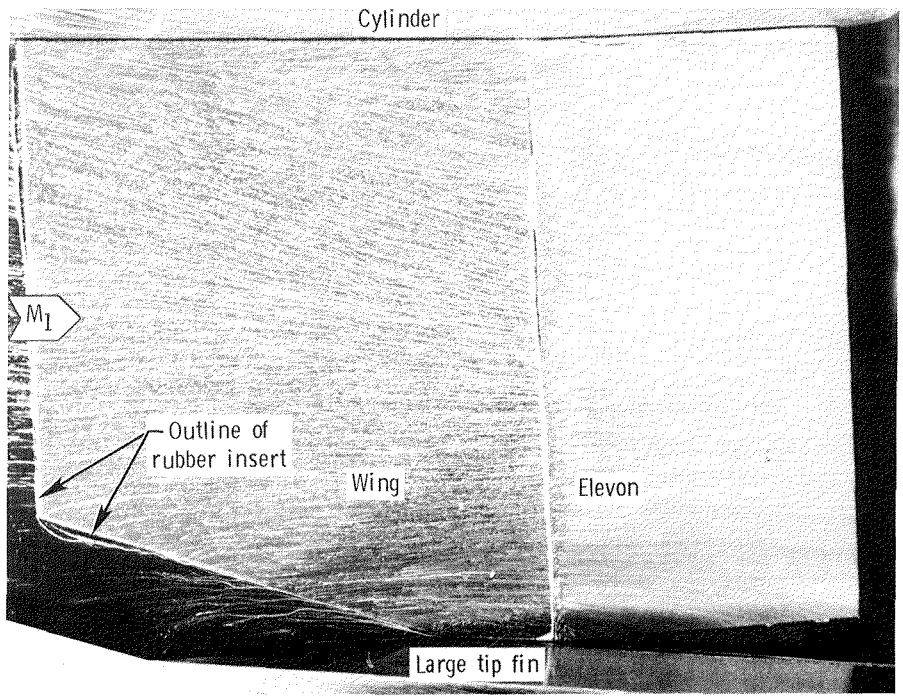

(a) Cylindrical body and tip fin. $\epsilon = 20^{\circ}$.

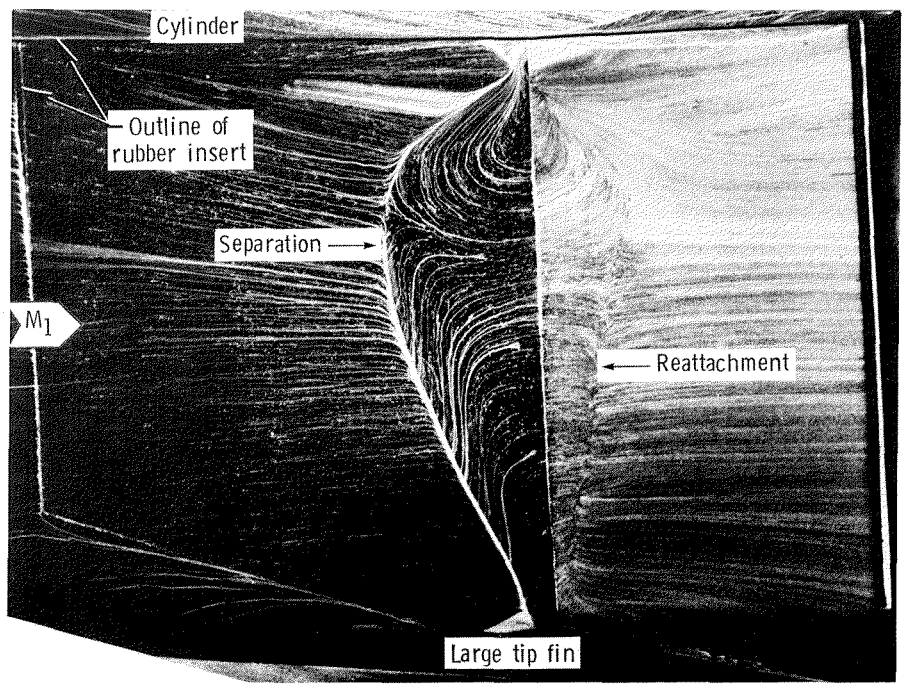

(b) Cylindrical body and tip fin. $\epsilon = 30^{\circ}$.

L-81-165

Figure 6.- Planform oil-flow pictures for 70° swept wing with various attachments and elevon deflection angles. $M_1 = 5.9$.

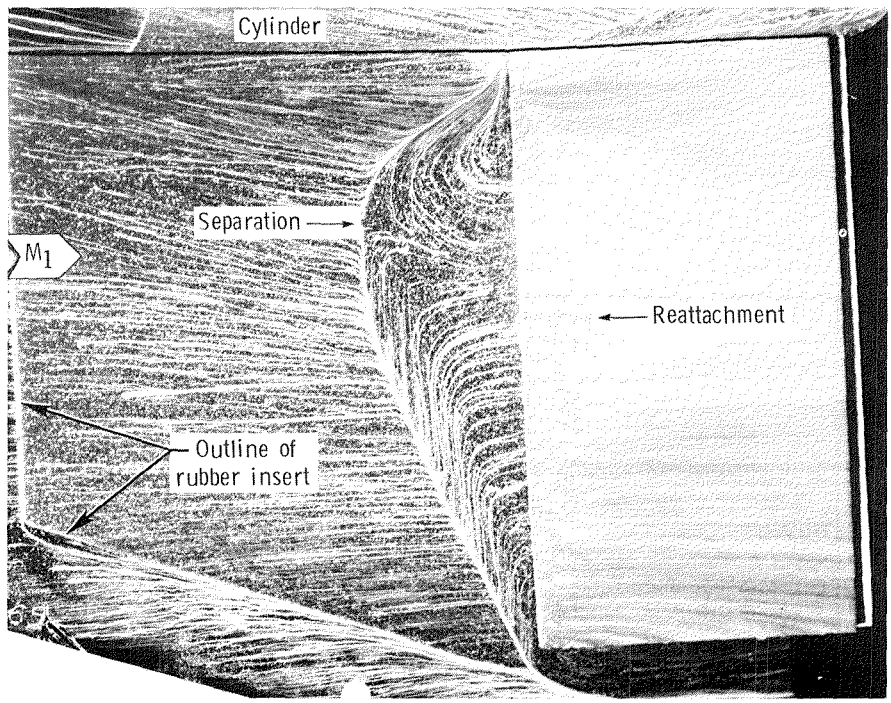

(c) Cylindrical body. $\varepsilon = 30^{\circ}$; no tip fin.

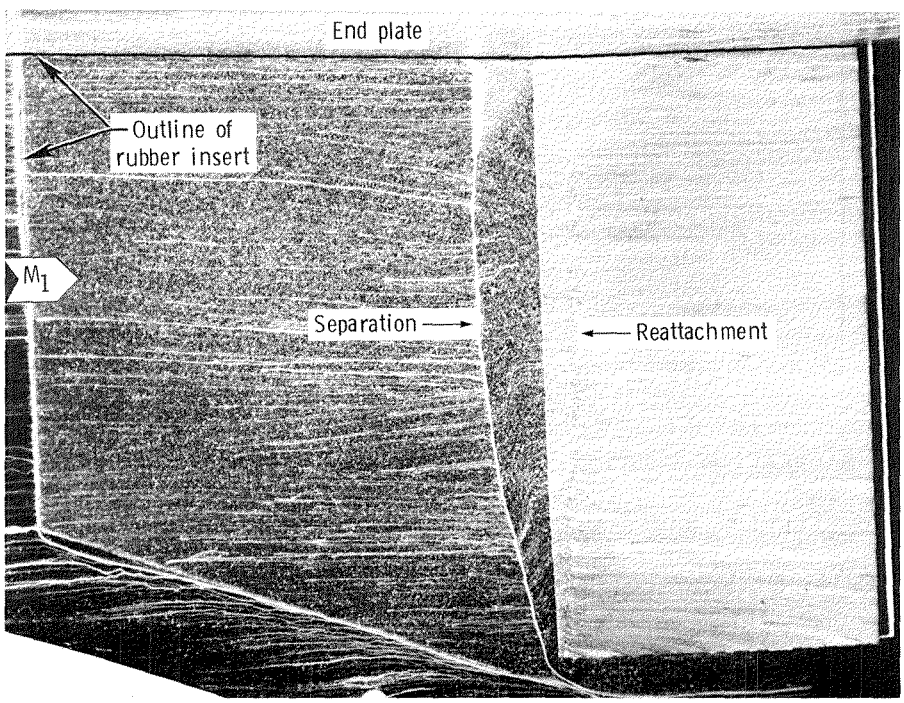

(d) End plate. $\varepsilon = 30^{\circ}$; no tip fin.

L-81-166

Figure 6.- Concluded.

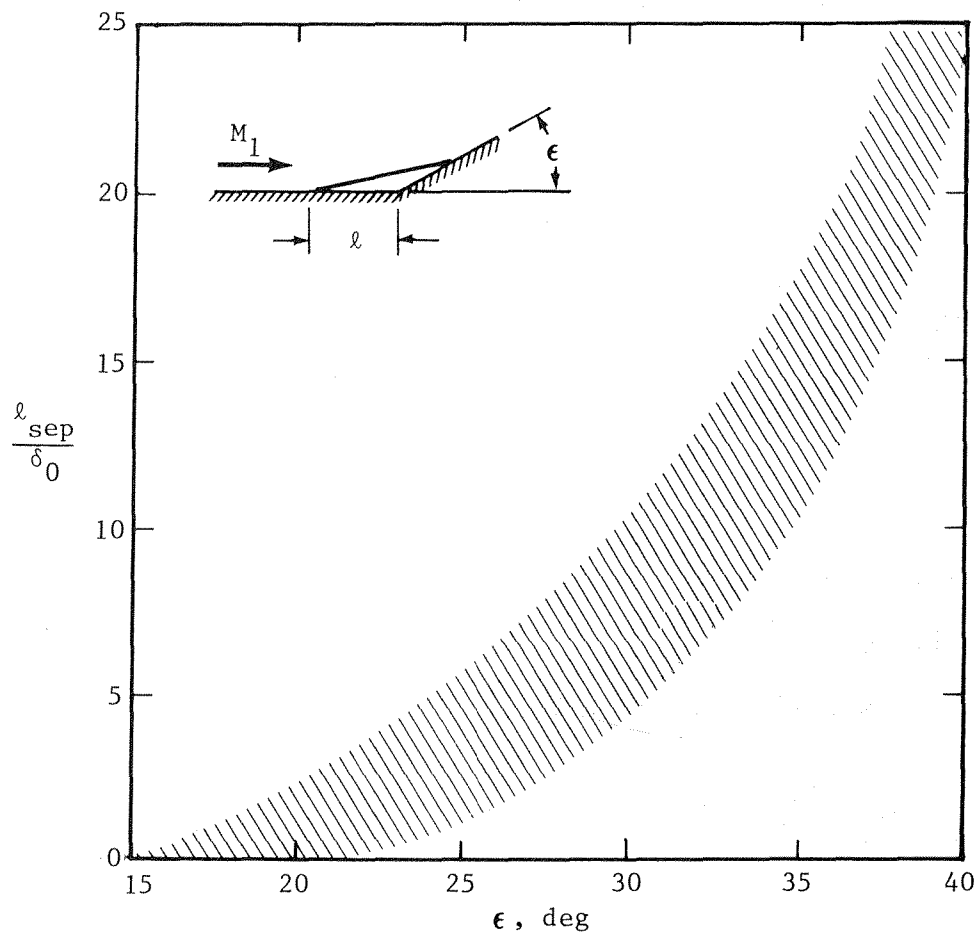

Figure 7.- Separation lengths ahead of trailing-edge flaps. Values of ℓ_{sep}/δ_0 increase with decreasing M_1 and R for a specific elevon deflection angle.

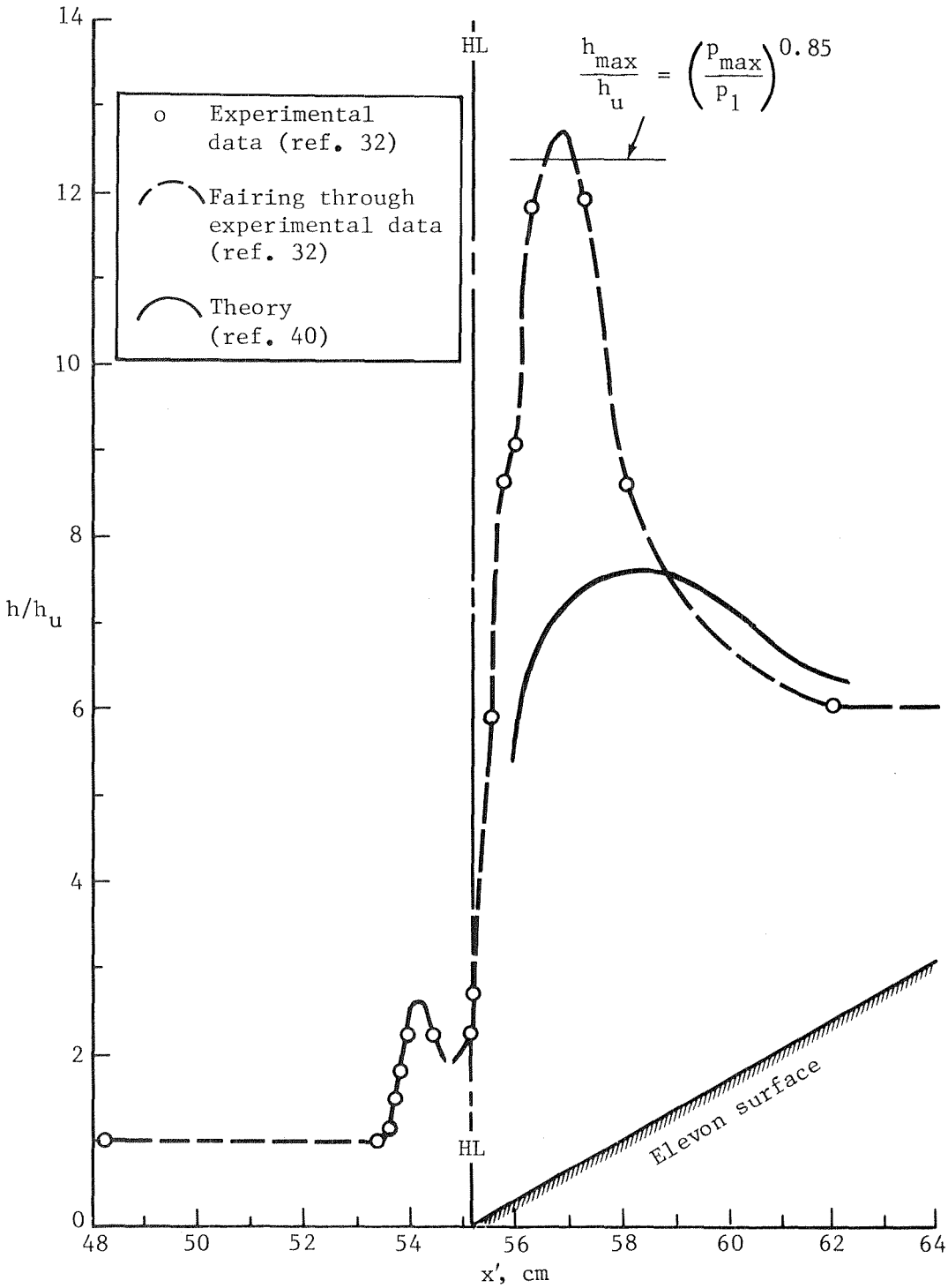

Figure 8.- Streamwise distributions of heat-transfer-coefficient ratios on unswept wing and 30° elevon surfaces for $M_1 = 5.9$.

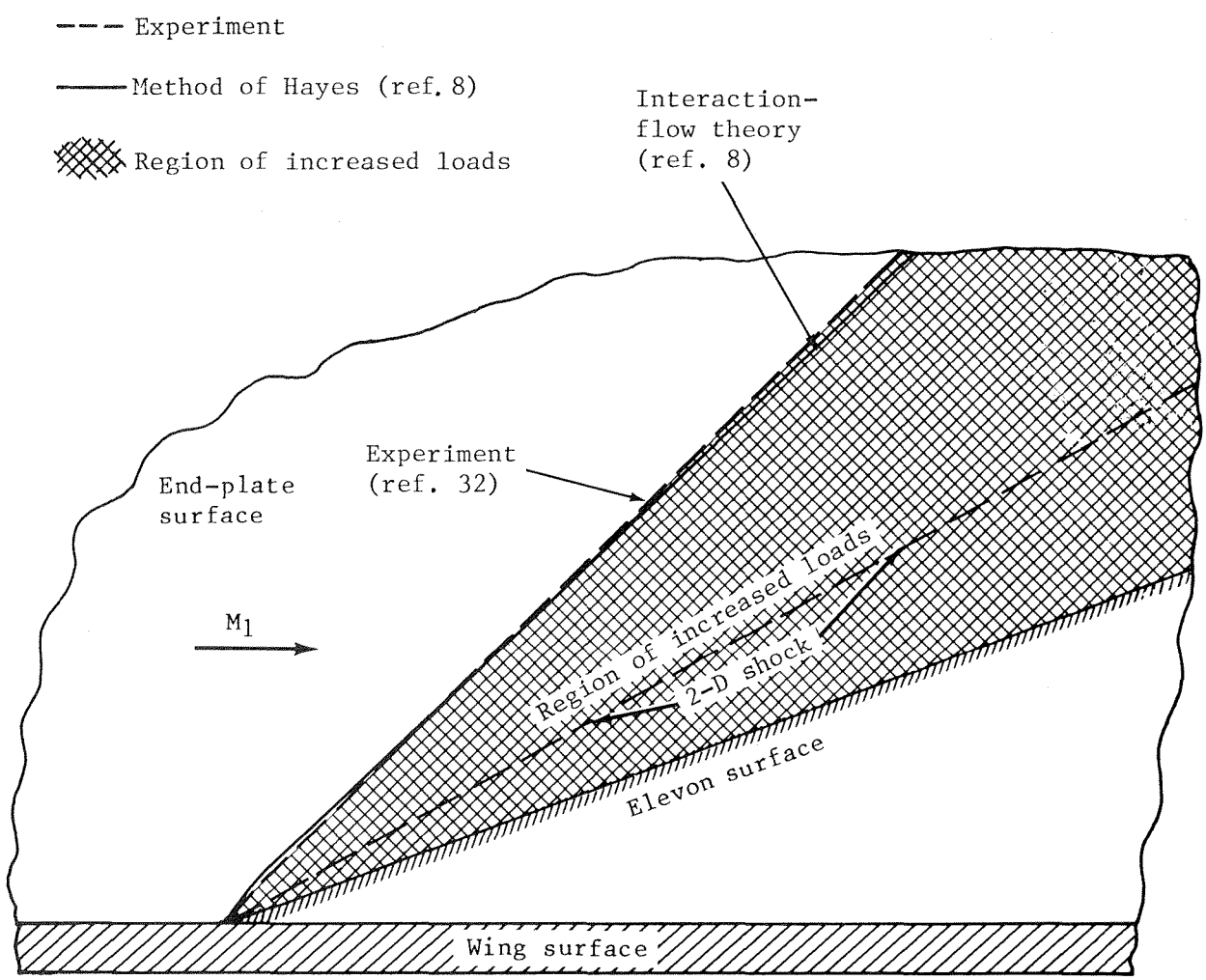

Figure 9.- Region of increased pressure and thermal loads on end-plate surface for $M_1 = 5.9$ and $\varepsilon = 20^{\circ}$.

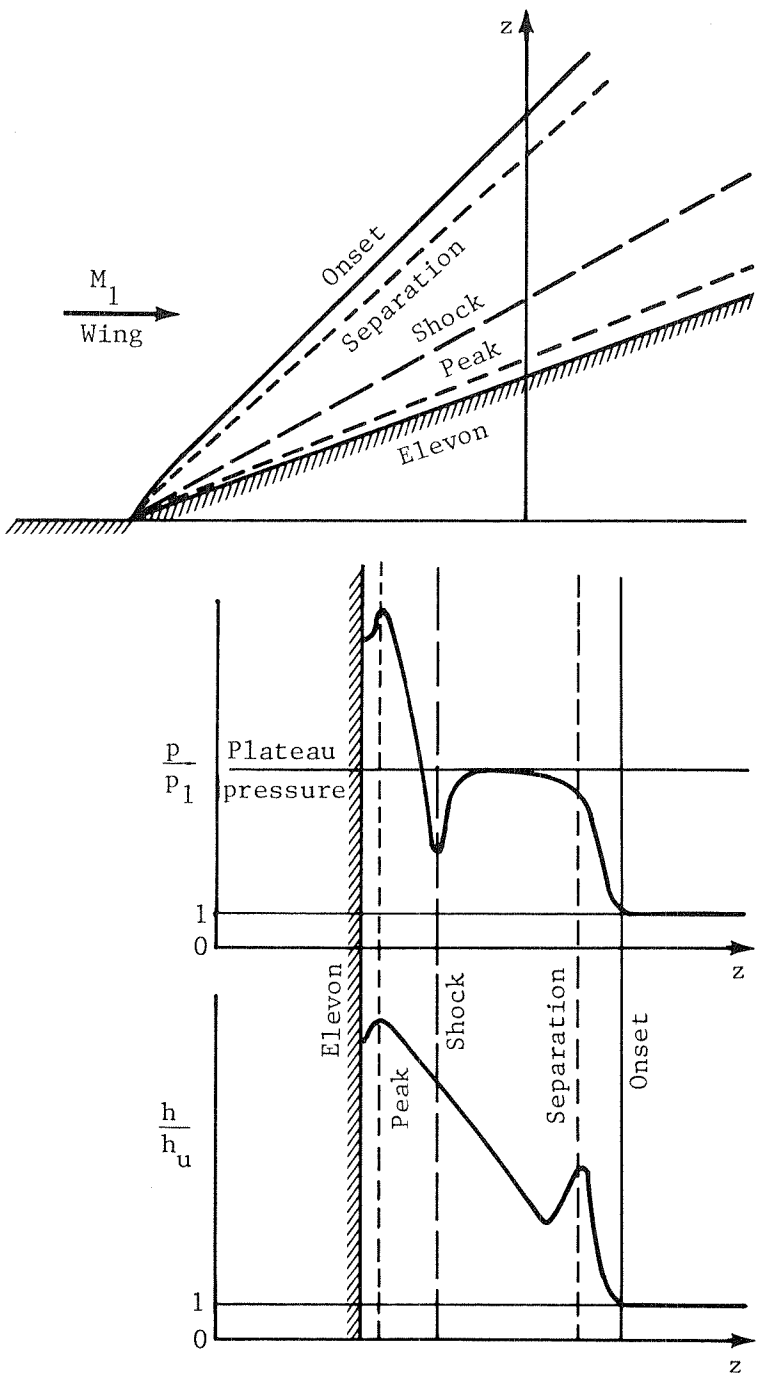

Figure 10.- Sketches of pressure and heat-transfer-coefficient distributions in interaction-flow region (from ref. 8).

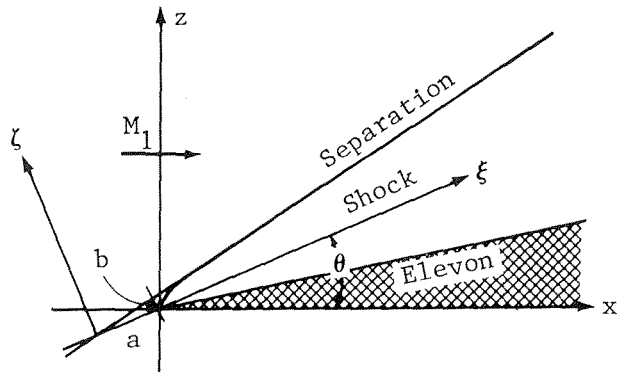

(a) No flow separation upstream of hinge line.

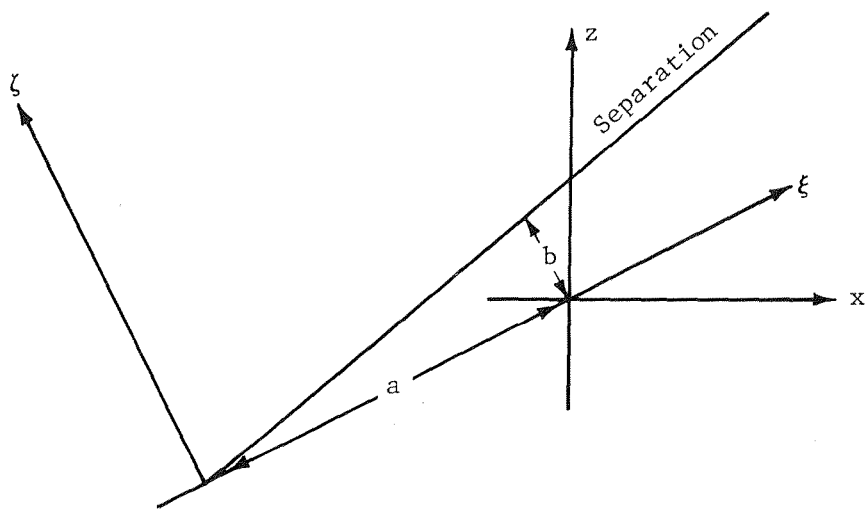

(b) Origins of coordinate systems.

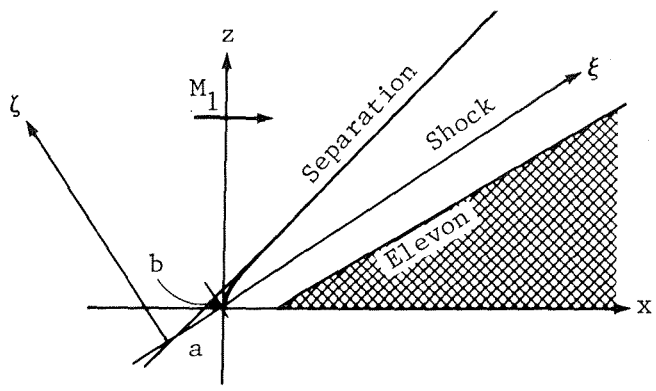

(c) Flow separation upstream of hinge line.

Figure 11.- Shock-oriented coordinate system.

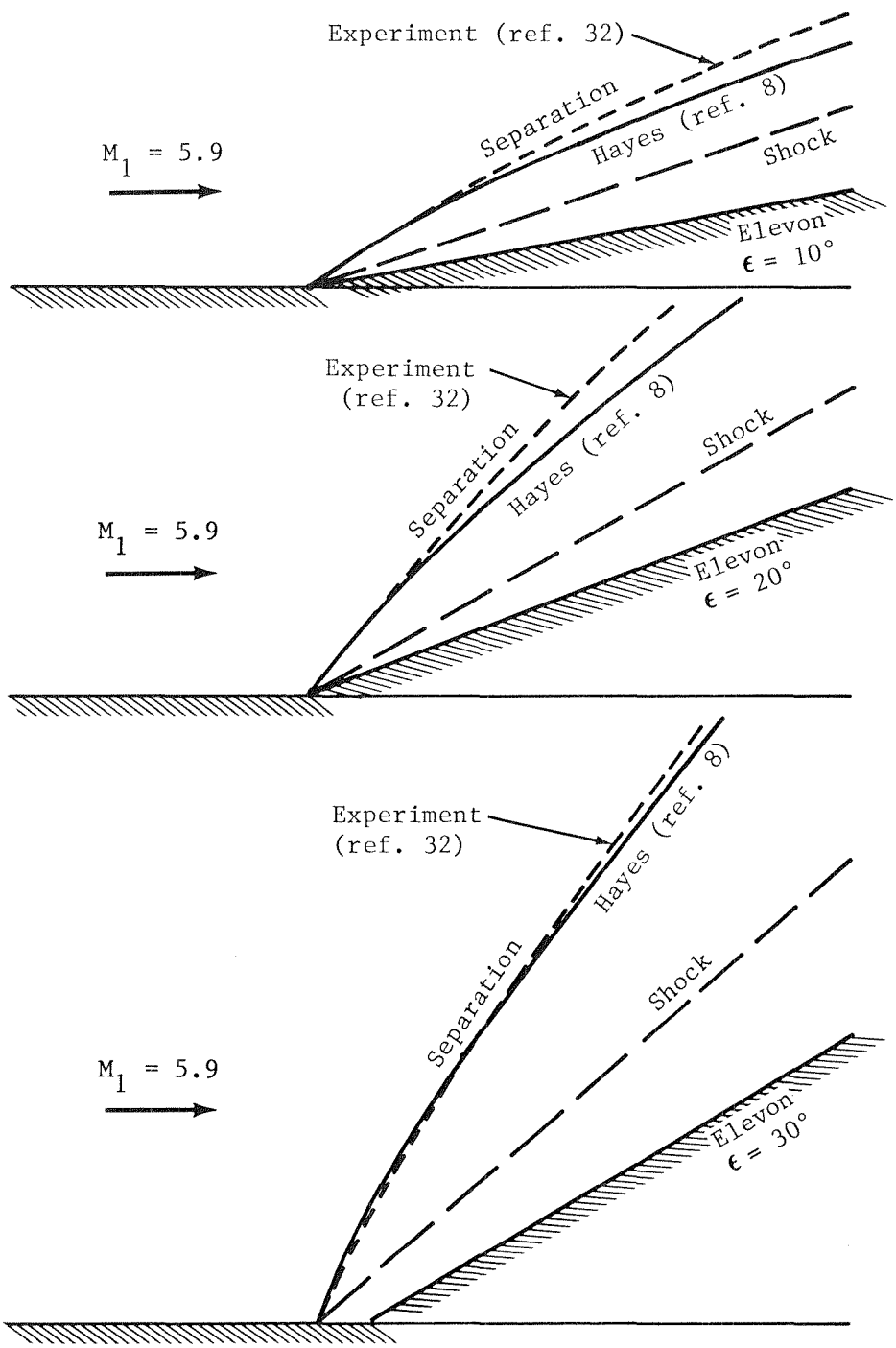

Figure 12.- Comparison of experimental observations of separation with analytical predications made using Hayes' method (ref. 8).

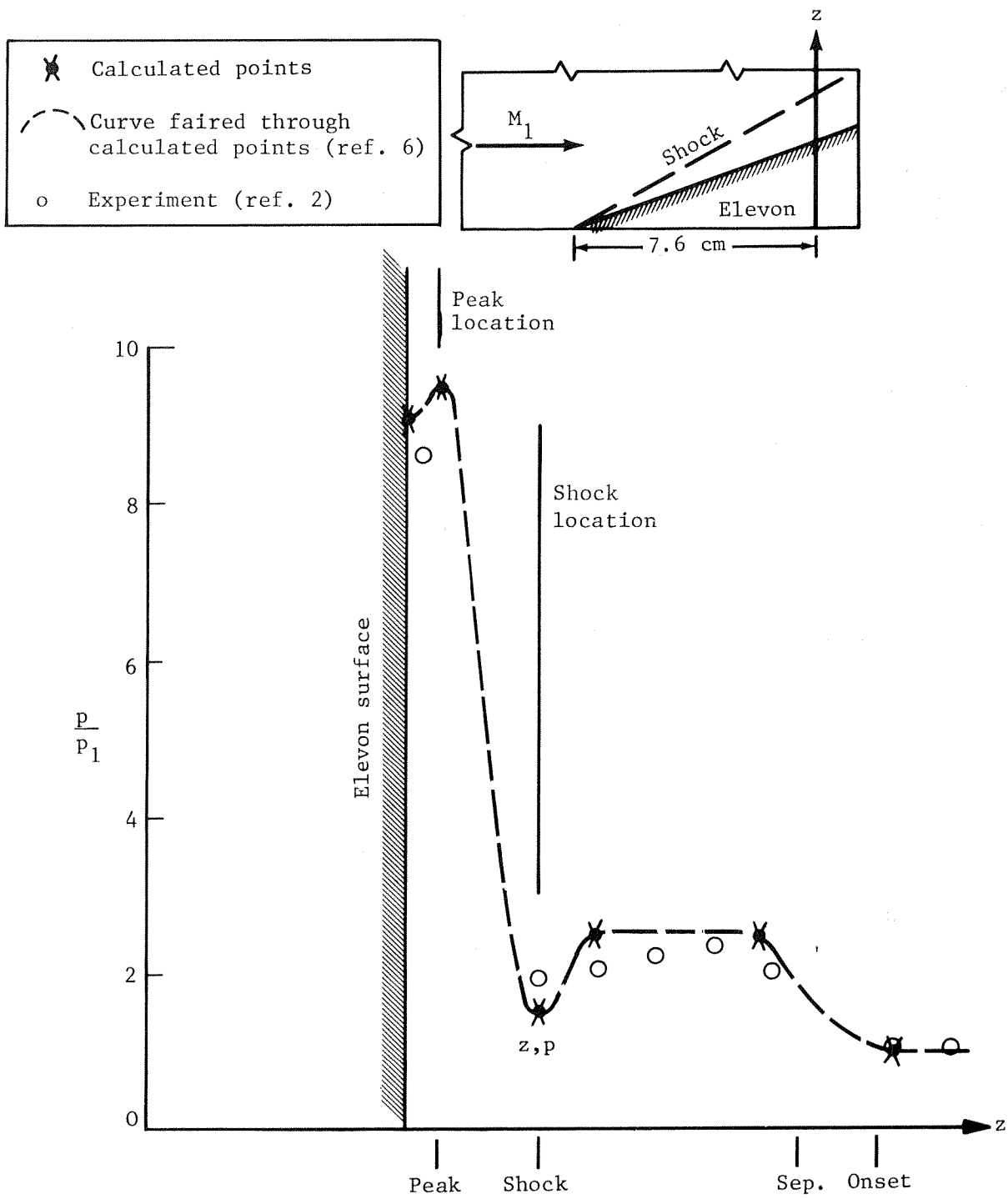

Figure 13.- Sample comparison of pressure distributions calculated using analytical method (ref. 8) with experimental data (ref. 2) for $M_1 = 5.9$ and $\varepsilon = 20^{\circ}$ at a station 7.6 cm downstream of elevon hinge line.

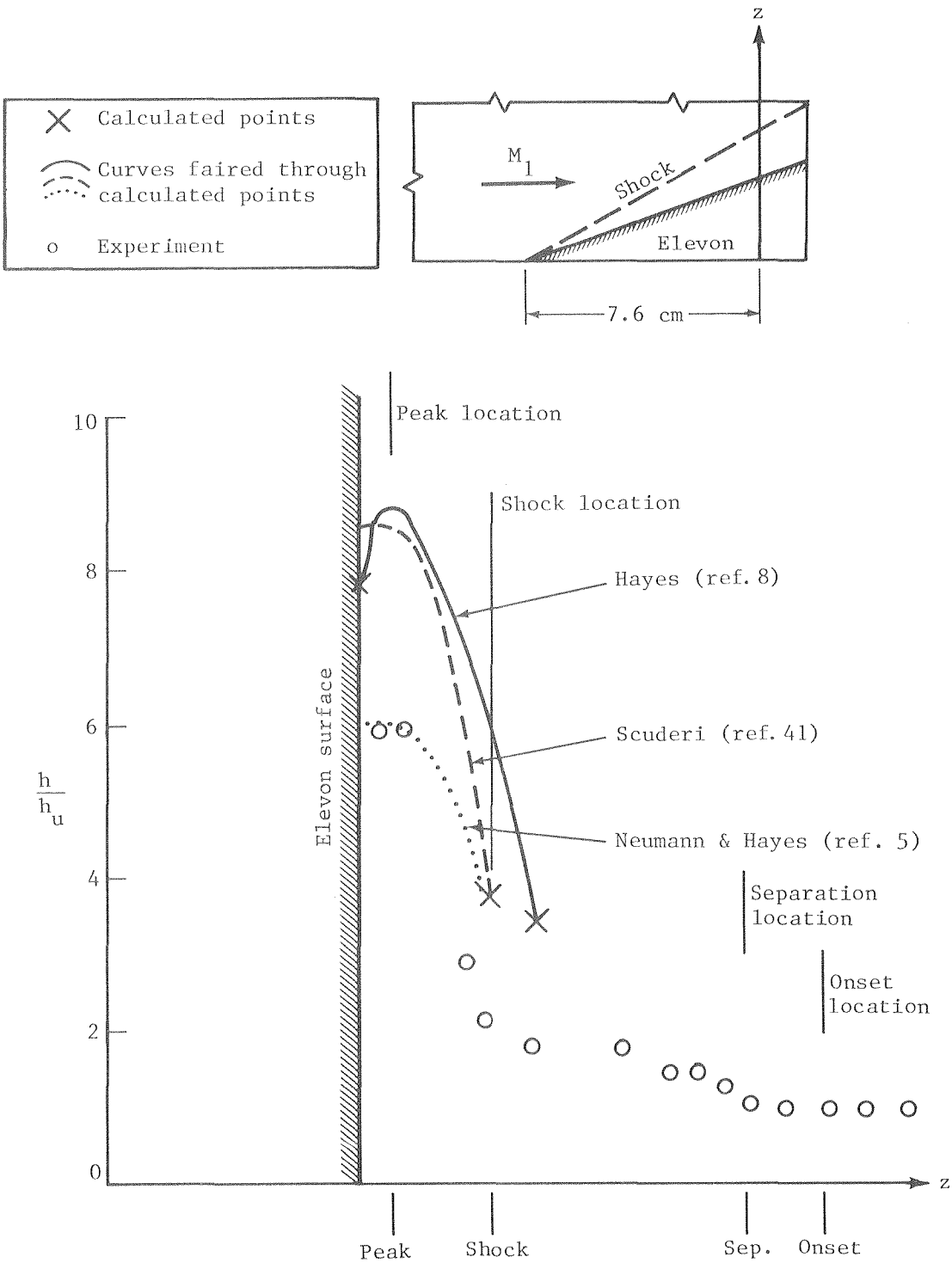

Figure 14.- Sample comparisons of peak heat-transfer coefficients for $M_\infty = 5.9$ and $\varepsilon = 20^\circ$.

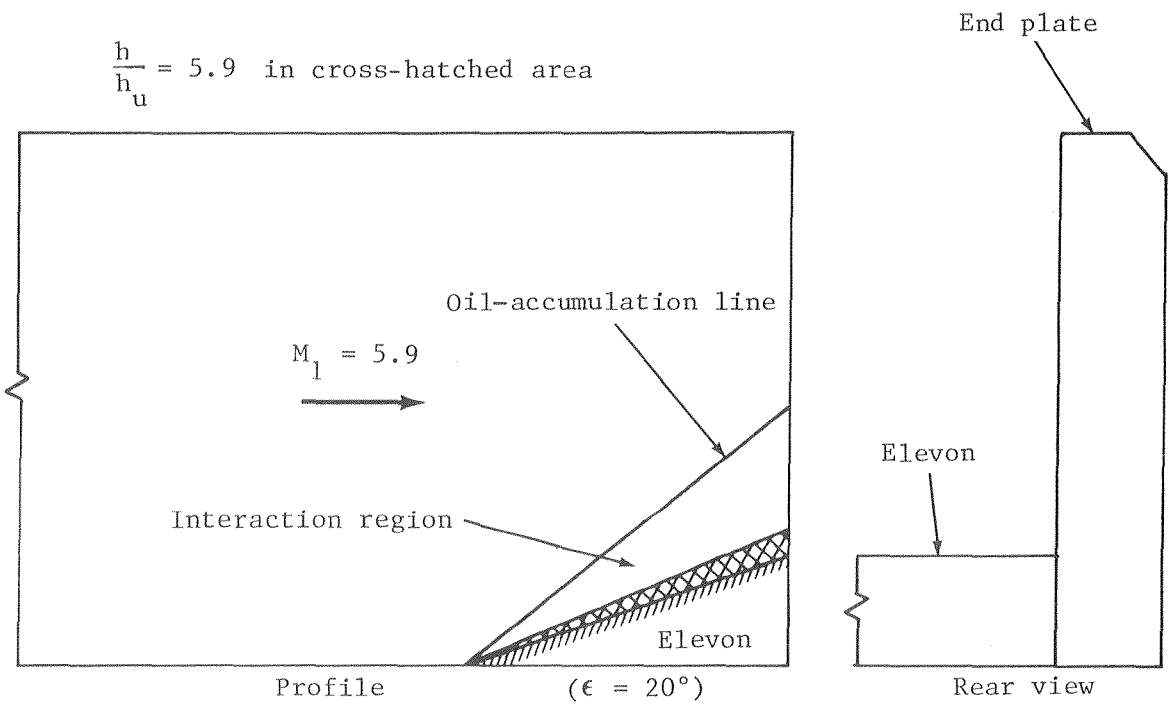

Figure 15.- Extent of interaction flow and region of high heating on end-plate surface.

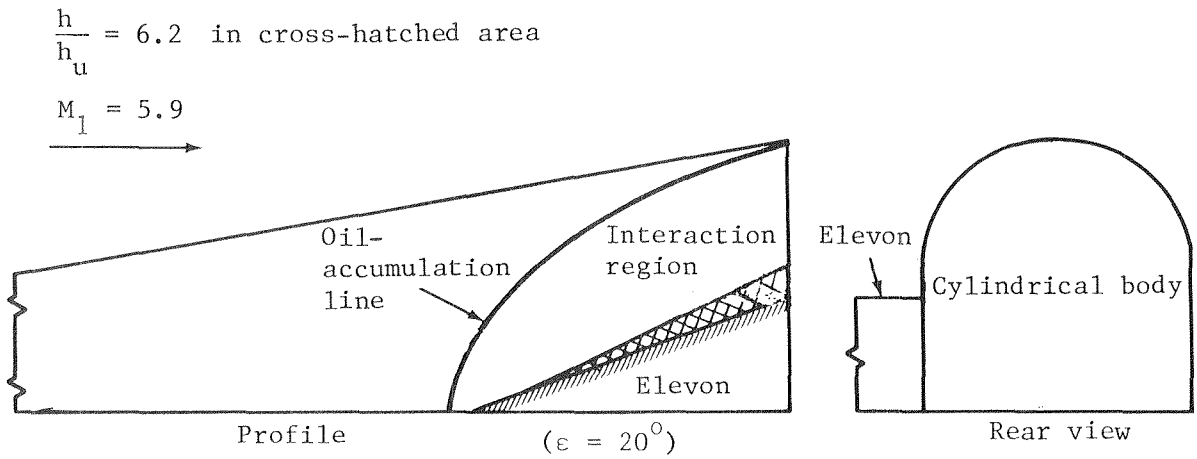

Figure 16.- Extent of interaction flow and region of high heating on cylindrical-body surface.

1. Report No.	2. Government Accession No.	3. Recipient's Catalog No.
NASA TM-83130		

4. Title and Subtitle	5. Report Date
METHODS FOR ESTIMATING PRESSURE AND THERMAL LOADS INDUCED BY ELEVON DEFLECTIONS ON HYPERSONIC-VEHICLE SURFACES WITH TURBULENT BOUNDARY LAYERS	September 1981
	6. Performing Organization Code 505-31-73-01

7. Author(s)	8. Performing Organization Report No.
Louis G. Kaufman II and Charles B. Johnson	L-14204
	10. Work Unit No.

9. Performing Organization Name and Address	11. Contract or Grant No.
NASA Langley Research Center Hampton, VA 23665	
	13. Type of Report and Period Covered Technical Memorandum

12. Sponsoring Agency Name and Address	14. Sponsoring Agency Code
National Aeronautics and Space Administration Washington, DC 20546	

15. Supplementary Notes

16. Abstract

Empirical-analytic methods are presented for calculating thermal and pressure distributions in three-dimensional, shock-wave, turbulent-boundary-layer, interaction-flow regions on the surface of controllable hypersonic aircraft and missiles. The methods, based on several experimental investigations, are useful and reliable for estimating both the extent and magnitude of the increased thermal and pressure loads on the vehicle surfaces.

17. Key Words (Suggested by Author(s))	18. Distribution Statement
Hypersonic flow Heat transfer Turbulent boundary layer Viscid-inviscid interaction Flow separation Pressure distributions	Unclassified - Unlimited Subject Category 34

19. Security Classif. (of this report)	20. Security Classif. (of this page)	21. No. of Pages	22. Price
Unclassified	Unclassified	40	A03

For sale by the National Technical Information Service, Springfield, Virginia 22161

NASA-Langley, 1981

End of Document